

## Central Lancashire Online Knowledge (CLoK)

Title	Cu-MOF loaded chitosan based freeze-dried highly porous dressings with anti-biofilm and pro-angiogenic activities accelerated Pseudomonas aeruginosa infected wounds healing in rats
Type	Article
URL	<a href="https://clock.uclan.ac.uk/51641/">https://clock.uclan.ac.uk/51641/</a>
DOI	<a href="https://doi.org/10.1016/j.ijbiomac.2024.132443">https://doi.org/10.1016/j.ijbiomac.2024.132443</a>
Date	2024
Citation	Zulfiqar, Saima, Sharif, Shahzad, Nawaz, Muhammad Shahbaz, Shahzad, Sohail Anjum, Bashir, Muhammad Mustehsan, Iqbal, Tariq, U Rehman, Ihtesham and Yar, Muhammad (2024) Cu-MOF loaded chitosan based freeze-dried highly porous dressings with anti-biofilm and pro-angiogenic activities accelerated Pseudomonas aeruginosa infected wounds healing in rats. International Journal of Biological Macromolecules, 271 (Pt 2). ISSN 0141-8130
Creators	Zulfiqar, Saima, Sharif, Shahzad, Nawaz, Muhammad Shahbaz, Shahzad, Sohail Anjum, Bashir, Muhammad Mustehsan, Iqbal, Tariq, U Rehman, Ihtesham and Yar, Muhammad

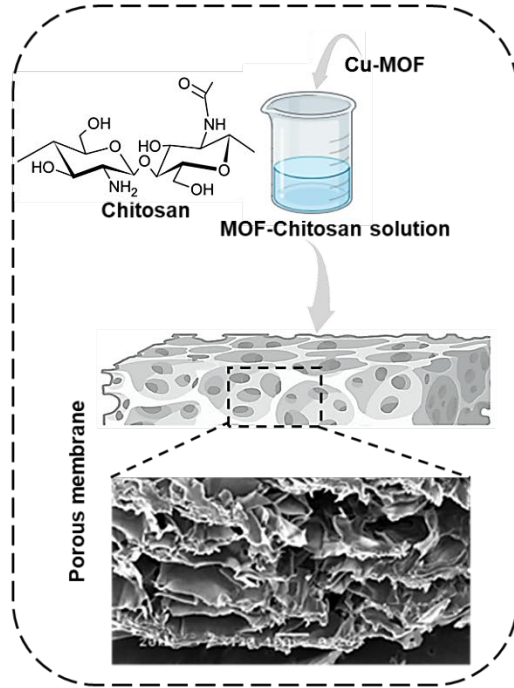
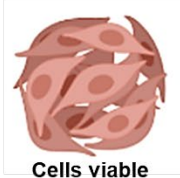
It is advisable to refer to the publisher's version if you intend to cite from the work.  
<https://doi.org/10.1016/j.ijbiomac.2024.132443>

For information about Research at UCLan please go to <http://www.uclan.ac.uk/research/>

All outputs in CLoK are protected by Intellectual Property Rights law, including Copyright law. Copyright, IPR and Moral Rights for the works on this site are retained by the individual authors and/or other copyright owners. Terms and conditions for use of this material are defined in the <http://clock.uclan.ac.uk/policies/>

# Graphical abstract

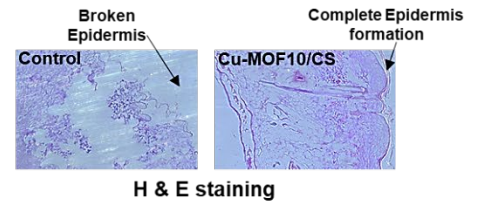
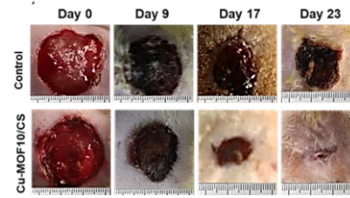
## In Vitro studies



## In Vivo studies



### *P. aeruginosa* Infected rat model



**Cu-MOF loaded chitosan based freeze-dried highly porous dressings with anti-biofilm and pro-angiogenic activities accelerated *Pseudomonas aeruginosa* infected wounds healing in rats**

Saima Zulfiqar<sup>1,2</sup>, Shahzad Sharif<sup>2\*\*</sup>, Muhammad Shahbaz Nawaz<sup>1</sup>, Sohail Anjum Shahzad<sup>3</sup>, Muhammad Mustehsan Bashir<sup>4</sup>, Tariq Iqbal<sup>5</sup>, Ihtesham ur Rehman<sup>6</sup>, Muhammad Yar<sup>1,\*</sup>

<sup>1</sup>Interdisciplinary Research Center in Biomedical Materials (IRCBM), COMSATS University Islamabad, Lahore Campus, Defence Road off Raiwind Road, Lahore 54000, Pakistan

<sup>2</sup>Department of Chemistry, Government College University Lahore Pakistan

<sup>3</sup>Department of Chemistry, COMSATS University Islamabad, Abbottabad Campus, University Road, Abbottabad 22060, Pakistan

<sup>4</sup>Department of Burns Surgery, King Edward Medical University, Mayo Hospital Lahore Pakistan

<sup>5</sup>Department of Burns Surgery, Shaheed Zulfiqar Ali Bhutto Medical University (SZABMU), PIMS, Islamabad, Pakistan

<sup>6</sup>School of Medicine, University of Central Lancashire, Preston, Lancashire PR1 2HE, United Kingdom

**Correspondence address:**

\*Dr Muhammad Yar, Interdisciplinary Research Centre in Biomedical Materials (IRCBM), COMSATS University Islamabad, Lahore Campus, Defence Road off Raiwind Road, Lahore 54000, Pakistan, Phone: 0092 42 111 001 007

E-mail: drmyar@cuilahore.edu.pk

\*\*Dr Shahzad Sharif, Department of Chemistry, Government College University Lahore Pakistan,

Phone: 0092-111-000-010 Ext. 44

E-mail: mssharif@gcu.edu.pk

## **Abstract**

Metal–organic frameworks (MOFs)-based therapy opens a new area for antibiotic-drug free infections treatment. In the present study, chitosan membranes (CS) loaded with two concentrations of copper-MOF 10mg/20ml (Cu-MOF10/CS) & 20mg/20ml (Cu-MOF20/CS) were prepared by a simple lyophilization procedure. FTIR spectra of Cu-MOF10/CS and Cu-MOF20/CS dressings confirmed absence of any undesirable chemical changes after loading Cu-MOF. The SEM images of the synthesized materials (CS, Cu-MOF10/CS & Cu-MOF20/CS) showed interconnected porous structures. Cytocompatibility of the materials was confirmed by fibroblasts cells culturing and the materials were hemocompatible, with blood clotting index <5%. Cu-MOF20/CS showed comparatively higher effective antibacterial activity against the tested strains; *E. coli* (149.2%), *P. aeruginosa* (165%) *S. aureus* (117.8%) and *MRSA* (142%) as compared to Amikacin, CS and Cu-MOF10/CS membranes. Similarly, Cu-MOF20/CS dressing significantly eradicated the biofilms; *P. aeruginosa* (37%) and *MRSA* (52%) respectively. In full thickness infected wound rat model, on day 23, Cu-MOF10/CS and Cu-MOF20/CS promoted wound healing up to 87.7% and 82% respectively. H&E staining of wounded tissues treated with Cu-MOF10/CS & Cu-MOF20/CS demonstrated enhanced neovascularization and re-epithelization along-with reduced inflammation, while trichrome staining exhibited increased collagen deposition. Overall, this study declares Cu-MOFs loaded chitosan dressings a multifunctional platform for the healing of infected wounds.

**Key Words:** Metal–organic frameworks (MOFs), Cytocompatibility, Biofilm, *P. aeruginosa*, neovascularization, collagen deposition, infected tissue regeneration

## **1. Introduction**

The largest organ in the human body is skin which is around 15% of total body weight and the 1<sup>st</sup> line of protection against infections. Around 20% of all illness and problems in human body are believed to be related to skin (1). Skin is highly susceptible to intentional (*e.g.*, surgery) or unintentional (*e.g.*, burns and abrasions) wounds, where bacterial infections lead to tissue damage, a significant inflammatory response, and a delay in wounds healing (2).

With two million cases of bacterial infections reported annually in USA alone, these pose a major threat to public health. At least 65% of these infections are linked to development of biofilms on mucous, tissues and medical implants which result in chronic wounds (3). Worldwide, mortality rate due to infection ranges from 20-40% (4). The treatment of bacterial wound infections has long involved the use of antibiotics that result in emergence of bacterial strains resistant to drugs, and decrease the efficacy of treatments against infected wounds (5). From individual to the healthcare and policymaker levels, treating and healing these wounds is very important from a social and economic perspective. In order to stop bacteria from spreading to the damaged area, wound dressings, that have good biocompatibility, permeability, tissue exudate absorbability and ease of removal are dressings of choice (6). But most of them do not possess antimicrobial ability to prevent wound infection (7). Thus, the development of ideal dressings capable of effectively managing infected wounds remains a challenge and therefore, the search for better antimicrobial strategies has become a topic of great concern (8).

Advanced wound dressings with promising healing abilities are highly desired. Fang Zhou et al., prepared zinc ions and ciprofloxacin-encapsulated chitosan/poly( $\epsilon$ -caprolactone) (CS/PCL) electrospun core-shell nanofibers and ciprofloxacin-functionalized PCL as the core and investigated their full thickness wounds healing activity (9). Zhang et al., prepared polyasparthydrazide (PAHy) nanofibers with different concentrations of *in-situ* synthesized silver nanoparticles (AgNPs) and these wound dressings exhibited antibacterial property, which make them a suitable candidate for infected wound healing (10). Li et al., prepared gelatin (Gel)/poly (L-lactic acid) (PLLA) nanofibrous with or without *Salvia miltiorrhiza* Bunge-*Radix Puerariae* herbal compound (SRHC), which were further interlaced into nanofibrous woven fabrics by modified electrospinning strategy. These bifunctional dressings showed potential for diabetic wound healing (11).

Antibacterial activity is essential for clinically used hydrogels, sponges and membranes to eliminate bacterial infections from wounds. Antimicrobial dressings have been prepared by using different antibiotics (12), which increase antibiotic resistance. Natural polysaccharide chitosan (CS) (13) possesses a number of inherent activities, such as muco-adhesion, biocompatibility, antimicrobial and excellent film forming ability (12, 14, 15). In order to promote blood coagulation and repair injured tissues, CS can provide active sites for blood cells (16). Furthermore, it has been observed that degradation of chitosan releases N-acetyl- $\beta$ -D-glucosamine which in turn promotes the growth of fibroblast cells and deposition of collagen, and ultimately stimulating wound healing process (17).

Metal organic frameworks (MOFs) are the emerging nanomaterials, which have coordination bonds joining metal ions/clusters as metal nodes and organic ligands as linkers (18, 19). MOFs are highly crystalline, hybrid and porous materials and have demonstrated promise for use in delivery

of protein, drugs, and genes (20-22) due to their tunable pore size as well as advanced physiochemical functionality (23), which make them suitable for biological applications (24-26). Due to wide range applications of MOFs, there has been a recent increase in interest in using them to promote skin regeneration and wound healing (27). Yuan et al., prepared MOF/cotton composite dressings by covering gauze with zinc based zeolitic imidazolate framework, to be used as microbicidal wound dressing (28). Huang et al., reported copper ( $\text{Cu}^{2+}$ ) and cobalt ( $\text{Co}^{2+}$ ) MOFs for wound healing with exceptional antibacterial activity and minimal toxicity (29). While, Yao et al., synthesized a hydrogel wound dressing utilizing the zeolitic imidazolate framework (ZIF-8) that facilitates the release of zinc ions ( $\text{Zn}^{2+}$ ), hence exhibiting antibacterial properties, growth of fibroblasts, collagen deposition, and angiogenesis (30).

Numerous studies have demonstrated remarkable antibacterial abilities of copper-based MOFs and their potential benefits for wound healing. These release copper ions more gradually and under control than copper NPs, which promotes healing while reducing the likelihood of copper precipitates that could harm natural organs. (31).

Considering the biological benefits of  $\text{Cu}^{2+}$ , we have prepared novel copper metal–organic frameworks (Cu-MOF), by a simple sono-chemical approach, and loaded into chitosan membranes for developing efficient biomaterials for wound healing. We examined their angiogenic potential by chorioallantoic membrane (CAM) assay, which has been tested first time to the best of our knowledge. Based on the limitations associated with antibiotics resistance, the current approach may offer a promising strategy for enhancing wound healing and addressing the clinical challenge of chronic wounds.

Since, it is of considerable interest to design a wound dressing that can prevent infection. The present study aimed to fabricate a Cu-MOF incorporated chitosan composite membrane via freeze

drying method. *In vitro* biocompatibility, antibacterial activity and angiogenic potential of the prepared composite membrane was comprehensively investigated. Finally, their ability to deal with severe wound infection and healing was evaluated by an infected wound rat model. This study provides a strategy for treating infected wounds and has potential of clinical translation.

## **2. Materials and Methods:**

Chitosan with molecular weight 50,000-190,000 Dalton, Copper (II) chloride dihydrate ( $\text{CuCl}_2 \cdot 2\text{H}_2\text{O}$ ) and dimethylformamide (DMF) were purchased from Sigma Aldrich, USA. Nutrient Broth and Nutrient Agar were obtained from Merck Chemical Co. Trypsin/EDTA solution (0.25%), Phosphate-buffered saline (PBS), Penicillin-Streptomycin (Pen-Strep), high-glucose content Dulbecco's Modified Eagle Medium (DMEM/HG), and fetal bovine serum (FBS) were supplied from GIBCO. Autoclaved deionized water was used to make all solutions. All chemicals and reagents used in experiments were of analytical grade.

### **2.1 Preparation of Copper metal organic framework**

Pyridine-2,4,6-tricarboxylic acid (52.8 mg, 0.25 mmol) was dissolved in 5 mL mixture of DMF and  $\text{H}_2\text{O}$  (20:80 v/v) and sonicated for 15 minutes at 15 microns amplitude and frequency of 23 KHz. Copper chloride (20.2 mg, 0.15 mmol) was dissolved in 1 mL of deionized water. Ligand and metal salt solutions were mixed and the resulting solution was sonicated for 3 minutes at 15 microns amplitude and frequency of 23 KHz. Green powder was obtained after one week. Resultant product was washed with deionized water and air dried.

### **2.2 Preparation of copper metal organic framework (Cu-MOF) loaded chitosan membranes**

Three different formulations were prepared. 1) **CS**: Chitosan solution was prepared by dissolving 0.6 g of CS in 20 ml solution of 1% acetic acid by stirring at room temperature for 24 hours. 2) **Cu-MOF10/CS**: after preparation of chitosan solution, 0.6 g of CS in 20 ml solution of 1% acetic acid at room for 24 hours, 10mg Cu-MOF was added, and the solution was stirred at room temperature. After one hour, it was poured in petri plate. 3) **Cu-MOF10/CS**: 20mg Cu-MOF was added into 20 ml of chitosan (0.6 g of CS in 20 ml solution of 1% acetic acid) and this solution was poured into a petri plate (100mm by 15mm). All the petri plates were covered with aluminum foil and kept at -20°C freezer for 24 hours prior to freeze-dry. Then these were freeze dried at -105°C using a Labanco Freezone 4.5 L for 24 hours. These freeze-dried membranes were used for FTIR, SEM, cell culture tests, antioxidant, antibacterial and antibiofilm, CAM assay and animal studies.

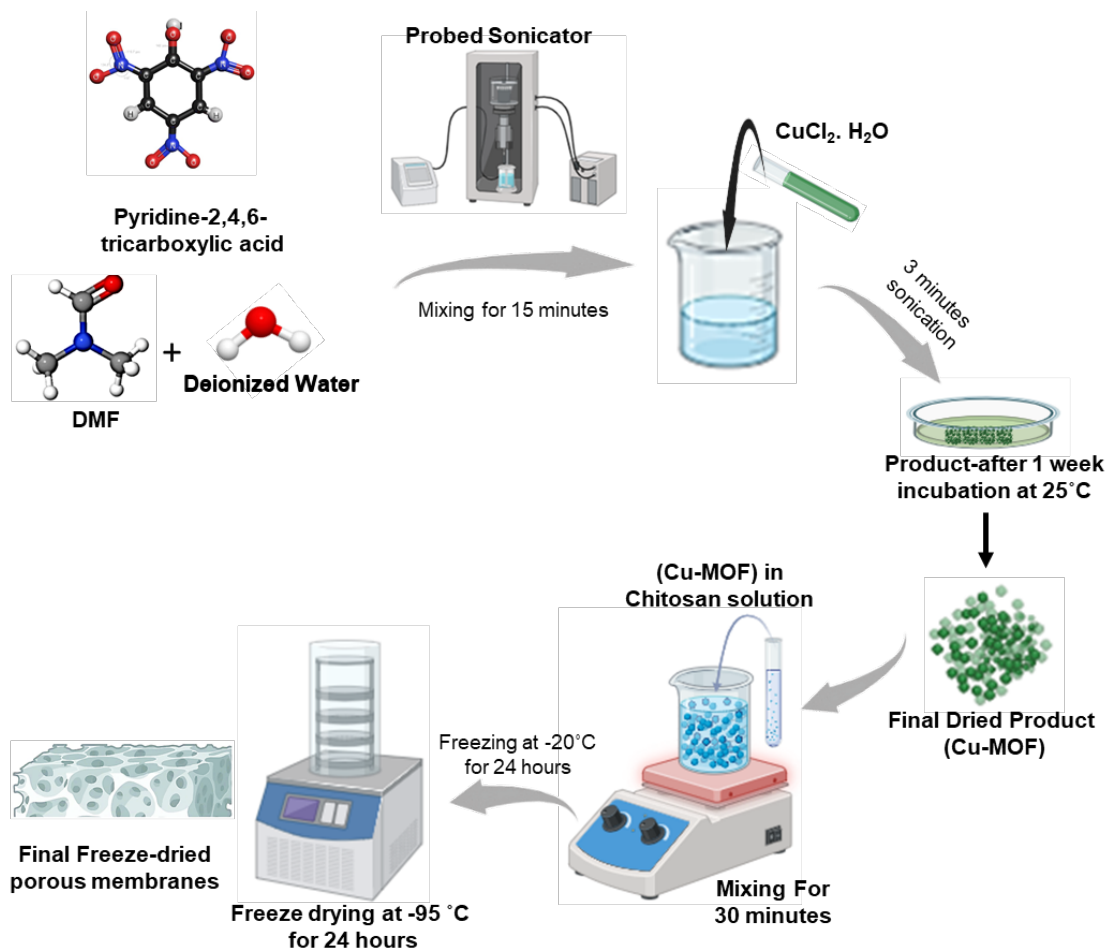


**Figure 1:** Synthesis scheme for preparation of Cu-MOF and Cu-MOF loaded chitosan membranes via Freeze drying method.

### 2.3 FTIR analysis

The chemical properties of freeze-dried membranes were evaluated using a spectroscopic analysis (FTIR) equipment in  $4000\text{--}400\text{ cm}^{-1}$  frequency range, 256 consecutive scans at  $8\text{ cm}^{-1}$ , and on smart mode (Thermo Nicolet 6700P spectrometer, Thermo Scientific, USA).

### 2.4 XRD analysis

Powder XRD analysis of Cu-MOF was performed by using XRD Shimadzu 6000 instrument. X-ray generator, operated at a voltage of 40 kV and a current of 30 mA, wherein the sample was subjected to Cu radiations at a step size of  $0.05^\circ$  and scanning of  $2\theta$  from  $15^\circ$  to  $80^\circ$ .

## **2.5 Scanning electron Microscope**

The morphology and microstructure of the freeze-dried membranes was investigated using a scanning electron microscope (TESCAN, VEGA LMU, Czech Republic). For this, a fragment of the samples was coated with a thin layer of gold. By measuring ten randomly chosen pores in the cross section, the pore size was determined using Image J (National Institutes of Health, Maryland, USA).

## **2.6 Swelling ratio %**

The patches were weighed as  $10 \pm 1$  mg and marked as  $W_0$ . Then, these were submerged into PBS (Phosphate Buffer Saline, pH 7.4) and incubated at  $37^\circ\text{C}$ . After initial incubation of 1, 4, 24 and 48 hours, these were removed from PBS and carefully tapped with filter paper, weighed and marked as  $W_1$ . The following formula was used to determine the swelling ratio:

$$\text{Swelling Ratio \%} = (W_1 - W_0) / W_0$$

## **2.7 *In vitro* studies**

### **2.7.1 Cell Viability assay**

Mouse fibroblast cells (NIH-3T3) at passage 5 were used to test membranes for toxicity and safety, in cell culture experiments. For this, gamma sterilized  $0.5 \times 0.5 \text{ cm}^2$  freeze dried membranes (of equal dimensions) were used. In T75 flask, NIH-3T3 cells were cultured in DMEM supplemented with 10% fetal bovine serum and 1% Penicillin-Streptomycin. After trypsinization, 2000 cells

were seeded onto membranes (0.5 x 0.5cm<sup>2</sup>) in each well of 24 well plate, along-with the cells without membranes as control. Then, the plate was incubated at 37°C in an incubator with 5% CO<sub>2</sub>. To find percentage cells viability, on day 1, 3 and 7, a 100µl AlamarBlue solution was added into each well and after 4 hours incubation, the optical density was recorded at 590 nm. The experiment was performed in triplicates. Cell viability against the synthesized membranes was calculated by:

$$\text{Cell viability} = (A_{\text{Sample}} - A_{\text{Blank}} / A_{\text{Control}} - A_{\text{Blank}}) 100$$

Where  $A_{\text{treatment}}$  is the absorbance of cells with membranes,  $A_{\text{control}}$  is the absorbance of cells and  $A_{\text{Blank}}$  is the absorbance of cell media.

### 2.7.2 In vitro blood compatibility assay

To assess the blood biocompatibility, a procedure was adopted as reported in literature (32), rat citrated blood was diluted with saline (Saline: Blood; 5:4). 1ml of this diluted blood was added onto 1 x 1cm<sup>2</sup> patches of the freeze-dried membranes in triplicate and incubated for 1 hour at 37°C. Normal saline treated red blood cells was used as control. Following 5 minutes centrifugation at 1000RPM, 100 µl supernatant was poured into 96 well plate and OD was measured at 540 nm using a microplate reader. The following formula was used to determine the % hemolysis:

$$\% \text{Hemolysis} = (OD_s - OD_B / OD_C - OD_B) 100$$

Where  $OD_s$ ,  $OD_B$  and  $OD_C$  are the optical density of sample, blank (Normal saline treated with RBCs as negative control) and Control (distilled water treated with RBS as positive control) respectively.

### 2.7.3 Blood clotting index (BCI)

The freeze-dried membranes were cut into 1 x 1cm<sup>2</sup> pieces in triplicate and placed onto glass plate to assess BCI value (32). A 100µl fresh rat blood was progressively added to cover the membranes and incubated for 5 minutes at 37°C. The membranes were washed with deionized water and a 100µl pure blood in 10 ml deionized water was used as control. The plates were shaken for 10 minutes at 37°C and 30 RPM, and the absorbance was measured using microplate reader at 540 nm. Using the following formula, BCI value was calculated:

$$\% \text{ BCI} = (\text{OD}_s / \text{OD}_c) 100$$

Where OD<sub>s</sub> and OD<sub>c</sub> are the optical density of sample and control respectively.

### 2.7.4 Antioxidant assay:

DPPH test was used to assess how the freeze-dried membranes scavenged free radicals created. In 24 well plate, 10 mg of Cu MOF loaded and membranes (Cu-MOF10/CS and Cu-MOF20/CS) were soaked in PBS for 72 hours. Following addition of 2ml ethanol (100% pure) into each well, the well plate was incubated at 37°C for next 24 hours. Ascorbic acid was used as positive control. Then after centrifugation, 1ml of the previously prepared solutions were mixed with 4 mL of 0.1 mM DPPH solution. After 30 minutes room temperature incubation, the absorbance at 517nm was measured using a microplate reader. The following formula was used to calculate the radical scavenging activity.

$$\% \text{ Radical scavenging activity} = (\text{Ac}-\text{As}/\text{Ac})100$$

where Ac represents the absorbance of the control group and As represents the absorbance of the sample-treated groups.

### 2.7.5 Antibacterial Activity Analysis

Agar plate disk diffusion technique (33, 34) was employed to assess the antibacterial effect of the freeze-dried membranes (8mm discs), against Gram-negative (*Escherichia coli* and *Pseudomonas aeruginosa*) and Gram-positive bacteria (*Methicillin-resistant Staphylococcus aureus* and *Staphylococcus aureus*). Amikacin (aminoglycoside anti-biotic; 8mm disc) discs were used as positive controls and 8mm simple filter paper disks were used as negative controls. The agar surface was directly in contact with a 8.0 mm diameter disk-shape of each membrane. The procedure was carried out in triplicate. For this, all the four bacteria were grown in the sterilized nutrient broth at 37°C. After 24 hours, 100µl each bacterial strain having 0.1 optical density was equally distributed onto the nutrient agar plates. Membranes (8mm) were placed onto agar surface. Following 24-hour incubation period at 37°C, the inhibitory zones on the plates were measured.

The effective antibacterial activity (EAA) of the prepared samples were calculated based on the following equation:

$$\% \text{ EAA} = (\text{ZI} / \text{S}) 100$$

Where ZI is the zone of inhibition and S is sample surface area in contact to agar.

### 2.7.6 Antibiofilm assay

*P. aeruginosa* and *MRSA* biofilms were produced and their survivability against CS, Cu-MOF10/CS and Cu-MOF20/CS was assessed according to reported procedure (35). The bacterial cultures were produced by inoculating a single colony of bacteria into LB broth and these were incubated at 37 °C. After 20 hours, the inoculums were centrifuged, washed and resuspended in M9 media (for gram negative bacteria, M9 with 15 v/v% tryptic soy broth (TSB was used)) until optical density reached 0.1. A 100µl of the seeding solutions were added into 96 well plates with

the discs (8mm) of Gentamycin, CS, Cu-MOF10/CS and Cu-MOF20/CS and the plates were incubated at 37°C under static conditions for three days. Then unattached cells were washed out thrice with PBS. To measure viability of treated biofilms, 10 v/v% of AlamarBlue reagent was added into every well and incubated at 37°C for 4 hours. Fluorescence intensity was measured at wavelength ( $\lambda$ ) 590nm. Biofilm viability was assessed by equation:

$$\text{Biofilm viability} = (I_{\text{Sample}} - I_{\text{Blank}} / I_{\text{Control}} - I_{\text{Blank}}) 100$$

Where,  $I_{\text{Blank}}$  is the fluorescence intensity of only 10 v/v% of AlamarBlue cell viability reagent,  $I_{\text{Control}}$  is the fluorescence intensity of untreated biofilms and  $I_{\text{Sample}}$  fluorescence intensity sample treated biofilms.

#### **2.7.7 Assessment of angiogenesis using the Chorioallantoic membrane (CAM) assay**

CAM assay was used to evaluate the angiogenic effect of Cu-MOF loaded chitosan membranes, according to (36, 37). It was performed in an egg incubator, cleaned with 70% ethanol and disinfection solution, at 37°C in a 55% humid environment. On day 0, the eggs purchased from Grand Parent Hatchery, Lahore were washed with 20% ethanol and placed in incubator. Then, on 7<sup>th</sup> day of incubation, a rectangular 1cm<sup>2</sup> window was cut in egg shell and 0.5cm<sup>2</sup> gamma sterilized membranes were placed to the chorioallantoic membrane. The window was sealed using paper tape and parafilm and the eggs were put back in the incubator at 37°C in a 55% humidity. On day 14, the eggs were opened, the digital pictures of membranes on CAM were taken and the eggs were sacrificed. The pictures were used to assess the total number of blood vessels around the samples (Image J) and their angiogenic characteristics (fold change in blood vessel length, diameter, and number of junctions) using Angioquant software (Tampere University of Applied Sciences, Finland).

## 2.8 Animal studies

### 2.8.1 Development of infectious wound model in SD rats

In this experiment, 16 SD male rats weighing  $250 \pm 30$  g were bought from CEMB, Punjab University in Pakistan. The animals were housed in a perfect environment for one week at  $25 \pm 1^\circ\text{C}$  and 12 hours of light and dark at a PCRF (Pre-Clinical Research Facility) at CUI, Lahore campus that is adhered to the guidelines for the care and use of laboratory animals, approved by the CUI, Lahore Ethical Committee. The facility performed all animal research in compliance with these guidelines.

Studies on animals were conducted to assess the impact of Cu-MOF/CS on the healing of biofilm infected wounds. Ketamine (50 mg/kg body weight) and xylazine cocktail (12 mg/kg body weight) were used as intraperitoneal anesthetics in Sprague-Dwaley rats. Hair at dorsal side were removed by electrical clipper followed by washing of shaved area with 70% ethanol solution. Using curved eye scissors, a full thickness circular excision of  $2 \times 2 \text{cm}^2$  in diameter was made on rat dorsal side. A total of sixteen SD male rats were split into four groups at random ( $n = 4$ ): a normal control group (without any treatment), a CS group (simple chitosan), a Cu-MOF10/CS group and a Cu-MOF20/CS group. To cause infection, 20  $\mu\text{L}$  of  $10^9$  CFU/mL *P. aeruginosa* suspension was applied to each wound. After 72 hours, the infected wounds of all groups were washed with normal saline and covered with the synthesized membranes (CS, Cu-MOF10/CS and Cu-MOF20/CS). The cotton gauzes were applied with surgical tape, as secondary dressing. To evaluate the infection, swabs from wound sites were taken on day 0 and 23. On day 23, all the animals were euthanized by cervical dislocation followed by general anesthesia with ketamine and xylazine for tissue collection. Digital photos were captured with a DSLR camera on days 0, 9, 17, and 23. Area

of each wound measured by using image J software was used to calculate % wound healing rate. The percentage of the wound healing area was calculated using the following equation.

$$\text{Percentage healing rate of wounds} = [A_0 - A_T / A_0 * 100]$$

The initial wound area on day 0 is denoted by  $A_0$ , and the wound area at time T is denoted by  $A_T$ .

### 2.8.2 Histological analysis

Rat skin samples taken on day 23 from wound site of each group were preserved for 72 hours in 10% formaldehyde solution, embedded in paraffin and sectioned using a microtome into 5  $\mu\text{m}$  thick pieces (Leica, Germany). Sections were fixed onto glass slides and stained with H&E and Masson's trichrome (Sigma Aldrich, USA) according to the manufacturer instructions. The inverted optical microscope (IM-3, OPTIKA, Italy) was used for capturing the images of the tissue sections.

## 2.9 Statistical Analysis

Each experiment was carried out in triplicate and mean  $\pm$  S.D. was computed from data. Unpaired Student t test was carried out using Graph-Pad QuickCalcs (<https://www.graphpad.com/quickcalcs/ttest1.cfm>). Findings with p-value < 0.05 were deemed statistically significant.

## 3. Results

### 3.1 FTIR

The binding of copper with PTA was confirmed by using FTIR spectroscopy. The FT-IR results for the molecular structure characterization of the component parts of the pure Cu-MOF material are shown in Figure 2(A).

In this spectrum, the vibrations associated with O-H, C-H aromatic,  $\text{-COO}^-$  stretching and C-H bending are corresponding to the bands at 3364.08, 3077.19, 1420.06 and 814.93  $\text{cm}^{-1}$ . The absorption bands appearing at 1562.86 and 1047.79  $\text{cm}^{-1}$  are related to C-N. The characteristic peaks at 3364.08  $\text{cm}^{-1}$  and 3724.16  $\text{cm}^{-1}$  are due to acidic OH of carboxyl ( $\text{-COOH}$ ) group and crystalline water. The bands at 1620.14 and 1601.5  $\text{cm}^{-1}$  indicates the asymmetric stretching of carbonyl group (C=O), while bands at 1420.06–1266.44  $\text{cm}^{-1}$  indicate symmetric stretching of carboxyl group (C=O) (38). The formation of Cu-based MOF was confirmed by the observation of a distinctive peak at 730.18  $\text{cm}^{-1}$  corresponding to the Cu–O vibration mode (39). The additional sharp peaks seen at roughly 780.72  $\text{cm}^{-1}$  and 1398.15–1334.25  $\text{cm}^{-1}$  correspond to the pyridine rings' C–N bending and C=C stretching vibrations, respectively. The lowering in symmetric and asymmetric vibrations of carboxyl group (C=O) reveals the binding of pyridine-2,4,6-tricarboxylic acid (H3PTC) with copper (40).

FTIR spectra of chitosan (CS) is shown in figure 2(A). Intermolecular hydrogen bonds and O-H stretching are shown by a prominent band between 3279  $\text{cm}^{-1}$ . C-H stretching is responsible for the absorption peaks at 2921  $\text{cm}^{-1}$ . These indicate the presence of polysaccharides. The bands at 1628  $\text{cm}^{-1}$  (C=O stretching) and 1335  $\text{cm}^{-1}$  (amide III's C-N stretching) respectively confirmed the presence of residual N-acetyl groups. The narrow band at 1536  $\text{cm}^{-1}$ , which is indicative of amide II N-H bending. The primary amine's N-H bending is shown as a band at 1589  $\text{cm}^{-1}$ . The bands at 1449 and 1399  $\text{cm}^{-1}$  exhibited  $\text{CH}_2$  and  $\text{CH}_3$  symmetrical deformation. The absorption bands at 1154  $\text{cm}^{-1}$  represent the C-O-C stretching, while bands corresponding to C-O stretching are located at 1064 and 1023  $\text{cm}^{-1}$ . However, after loading of Cu-MOF into chitosan membranes, there was no change in the peaks of CS.

### 3.2 XRD analysis

Figure 2(B) displays Cu-MOF X-ray diffractogram. PXRD analysis revealed intense diffraction peaks at (400), (222), (402), (444), (420), (882), (773), (882), and (311) centered at  $2\theta$  of  $6.42^\circ$ ,  $12.7^\circ$ ,  $17.42^\circ$ ,  $22.74^\circ$ ,  $28.22^\circ$ ,  $39.50^\circ$ ,  $44.5^\circ$ , and  $57.5^\circ$  respectively.

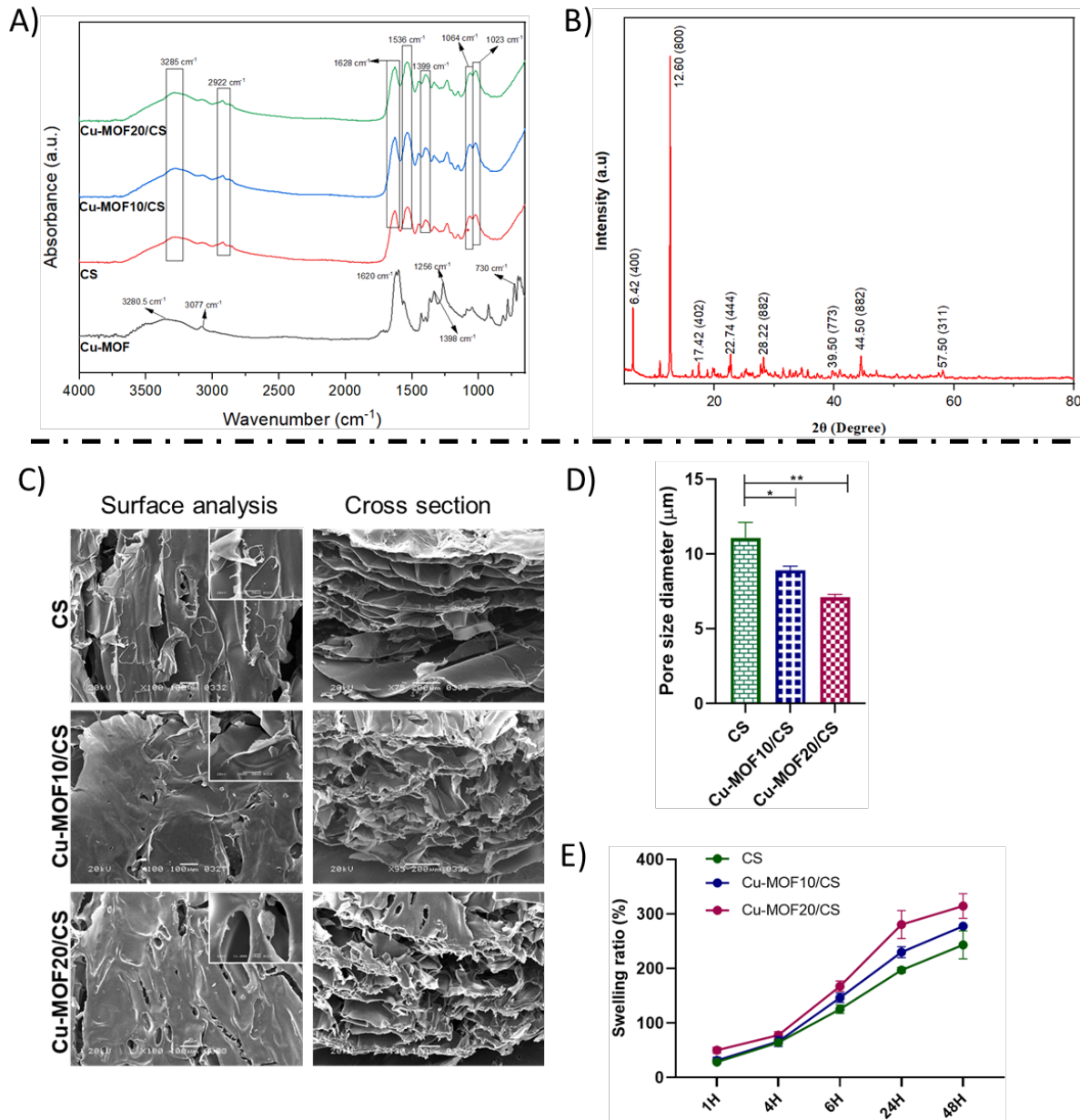


**Figure 2:** A) FTIR spectra of Cu-MOF, CS, Cu-MOF10/CS and Cu-MOF20/CS; B) XRD spectra of Cu-MOF; C) SEM images of CS, Cu-MOF10/CS and Cu-MOF20/CS at scale bar 100 $\mu$ m; D) Graph showing pore size; E) Swelling studies of Cu-MOF, CS, Cu-MOF10/CS and Cu-MOF20/CS in PBS solution at 1, 4, 6, 24 & 48 hours.

### 3.3 SEM analysis

Surface morphologies of freeze-dried membranes CS, Cu-MOF10/CS and Cu-MOF20/CS is shown in figure 2(C). SEM images of the samples clearly showed smooth membranes surface indicating homogenous blending of the MOF with chitosan. So, addition of copper metal organic framework did not change the surface properties of the chitosan. SEM images of cross sectioned membranes, as shown in figure 2(D), indicated a decrease in pore size diameter of membranes on increasing the concentration of Cu-MOF (10mg and 20mg/20ml) compared to CS. Calculated average pore size diameter of CS was 11.56  $\mu$ m and those of Cu-MOF10/CS and Cu-MOF20/CS was 9.27 and 7.17  $\mu$ m respectively.

### 3.4 Swelling ratio

Figure 2(E) shows the swelling ratios of samples in PBS. The results showed that the swelling ratio of CS increased by the incorporation of Cu-MOF. Cu-MOF10/CS, and Cu-MOF20/CS exhibited high capabilities in absorbing liquid compared to CS. It is shown that Cu-MOF20/CS beneficially increased the swelling ratio up to 312%. Pore size and large surface area of Cu-MOF may be responsible for this improved characteristic. It was observed that the swelling ratio of Cu-MOF20/CS was increased by about 30%. The obtained results indicated that high swelling ratio of CS membranes with Cu-MOF have ability to both absorb and shield the wound from fluid accumulation.

### 3.5 Cell Viability assay

The AlamarBlue assay was used to assess the viability of NIH-3T3 cells against CS, Cu-MOF10/CS and Cu-MOF20/CS, as shown in figure 3(A). All groups (Control, CS, Cu-MOF10/CS, and Cu-MOF20/CS) showed a consistent increase in percentage of cell viability, suggesting that cells were appropriately surviving and proliferating on the scaffolds. On day, 1, 3 and 7, it was observed that with the increase in Cu-MOF content from 10-20%, % cells viability values was increased for Cu-MOF10/CS and Cu-MOF20/CS. Overall, over 7-days incubation period, all tested materials showed no toxic effect towards cells.

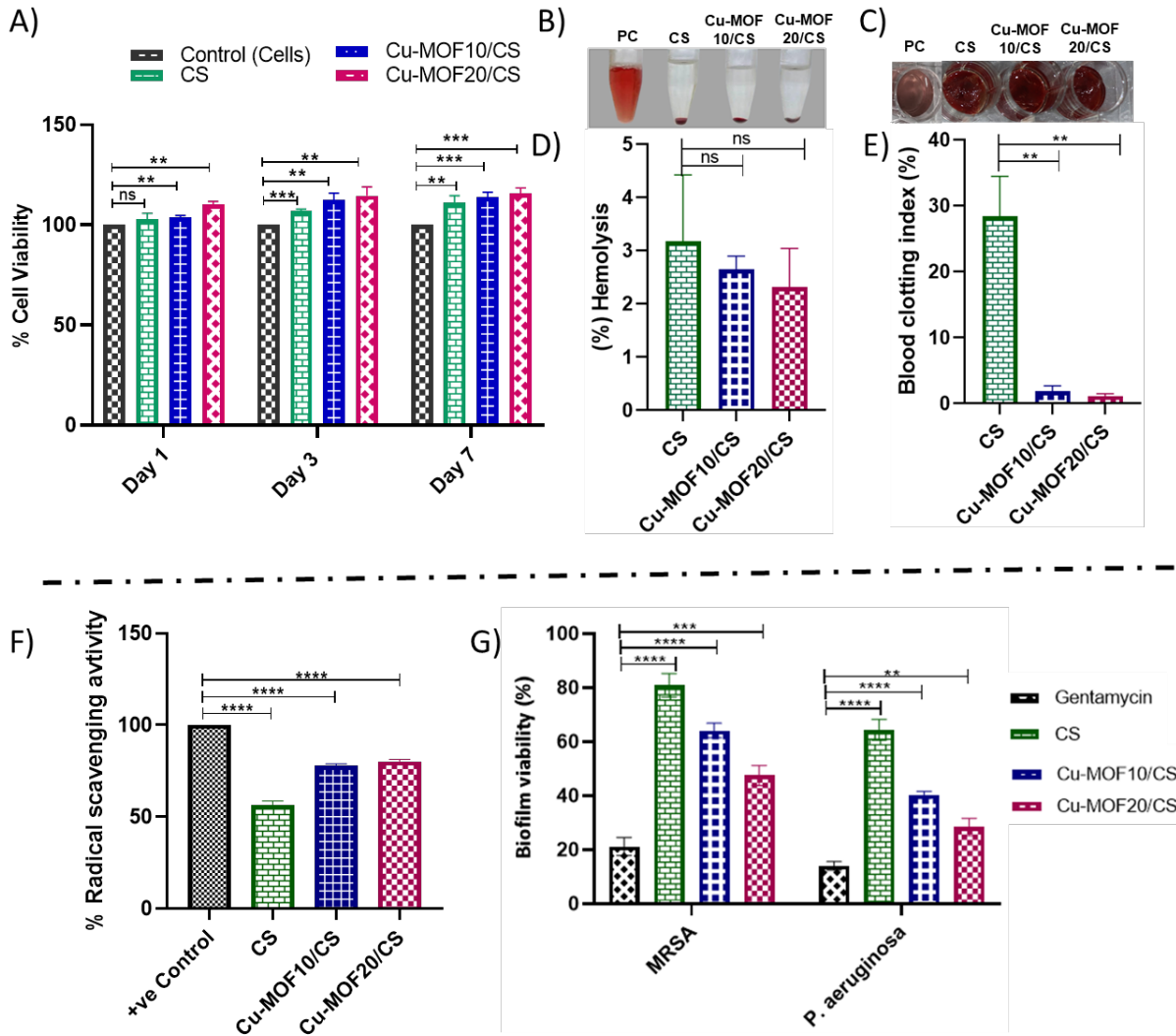


**Figure 3:** *In vitro* analysis of synthesized membranes (CS, Cu-MOF10/CS, and Cu-MOF20/CS). **A)** Cell viability of Control (Cells) and synthesized membranes for *in vitro* proliferation of fibroblast cells at different time intervals (Day 1, 3 & 7) Results are presented as n=3+SD. (on day 1,  $**P\leq 0.01$  denoted Control (cells) versus Control (Cells) versus Cu-MOF10/CS and Cu-MOF20/CS, while on day 3,  $***P\leq 0.001$  denoted Control (cells) versus CS &  $**P\leq 0.01$  denoted Control (cells) versus Cu-MOF10/CS, and Cu-MOF20/CS, while,  $**P\leq 0.01$  denoted Control (cells) versus CS &  $***P\leq 0.001$  denoted Control (cells) versus Cu-MOF10/CS, and Cu-MOF20/CS); **B)** The image of the clot and **C)** Hemolysis percentage of synthesized membranes ( $**P\leq 0.01$  denoted CS versus Cu-MOF10/CS & Cu-MOF20/CS); **D)** blood clotting index and **E)** The image of the clot before and after blood clot; **F)** DPPH assay for Synthesized membranes ( $****P\leq 0.0001$  denoted +ve control (Ascorbic acid) versus CS, Cu-MOF10/CS, and Cu-MOF20/CS); **G)** Biofilm viability of synthesized membranes against *P. aeruginosa* and MRSA ( $****P\leq 0.0001$  denoted Standard versus CS & Cu-MOF10/CS;  $**P\leq 0.01$  &  $***P\leq 0.001$  denoted Standard versus Cu-MOF20/CS).

### 3.6 Hemolysis Assay

Hemolysis was also evaluated by using rat blood, and the results were shown in Figure 3(B & C). Hemolysis ratios for CS, Cu-MOF10/CS, and Cu-MOF20/CS are 3, 2.78 and 2.316%. In the same manner, the macroscopic images of hemolysis assay revealed that Cu-MOF10/CS and Cu-MOF20/CS were somewhat yellow and control was bright red. According to findings, Cu-MOF10/CS and Cu-MOF20/CS exhibited good hemocompatibility.

### 3.7 Blood clotting index

As shown in figure 3(D & E) , the BCI (blood clotting index) of membranes was notably lower indicating that membranes rapidly absorbed the blood, increased blood viscosity, and promoted the aggregation of red blood cells and platelets.

In this study, the BCI value for the membranes reached  $23 \pm 1.12\%$ , indicating a weak function of this sample in forming a stable clot. The results indicated that the BCI values for developed CS,

Cu-MOF10/CS and Cu-MOF20/CS were 29, 1.2, and 0.9%, respectively. The minimum BCI index was achieved in Cu-MOF20/CS group, while the BCI value of water was 83.4%, in 10 min, which was the biggest of than other samples.

Figure 3(D& E) illustrates how blood clotting index (BCI) of membranes (Cu-MOF10/CS and Cu-MOF20/CS) was noticeably lower as compared to CS with a limited ability to form a stable clot, suggesting that they quickly absorbed blood, increased blood viscosity and encouraged aggregation of platelets and red blood cells.

### **3.8 Antioxidant assay**

In this study, the free radical DPPH scavenging ability of membranes was detected to evaluate the antioxidant performance of membranes. The present investigation assessed antioxidant potential of membranes by assessing their capacity to scavenge free radicals, via DPPH. Their antioxidant activity was compared with that of ascorbic acid (100%), the standard antioxidant. Figure 3(F) illustrates that following 30-minute incubation time, DPPH scavenging of CS was 52.4% primarily attributable to OH groups present in chitosan. After the addition of Cu-MOF into CS, the free radical scavenging rate of Cu-MOF10/CS, and Cu-MOF20/CS was increased to 75.5, and 78.7%. It was observed that with increase in concentration of Cu-MOF from 10-20%, the free radical scavenging rates were also increased.

### **3.9 Antibiofilm assay**

In this experiment, biofilms were inhibited by using Gentamycin (positive control), CS, Cu-MOF10/CS, and Cu-MOF20/CS, over 72 hours. These materials inhibited the biofilm formation upto 79, 81, 63 and 52) in case of *MRSA*, while 16.7, 62.1, 41 and 37% in case of *P. aeruginosa*. The results are shown in Fig. 3(G).

### 3.10 Antibacterial effect

Whereas CS, Cu-MOF10/CS, and Cu-MOF20/CS significantly inhibited the growth of *E. coli*, *P. aeruginosa*, *S. aureus*, and *MRSA*, as shown in figure (C & D). Cu-MOF10/CS showed 147.6%, 161.5%, 102.4% and 125.9% effective antibacterial activity (EAA) against *E. coli*, *P. aeruginosa*, *S. aureus*, and *MRSA* respectively. Whereas Cu-MOF20/CS exhibited 152.5%, 165, 117.8% and 142.1% % effective antibacterial activity (EAA) against *E. coli*, *P. aeruginosa*, *S. aureus*, and *MRSA* respectively. and 102% effective antibacterial activity (EAA) of CS. Overall, it is worth noting that Cu-MOF20/CS presented superior antibacterial effect against all these studied bacteria, consistent with literature (41).

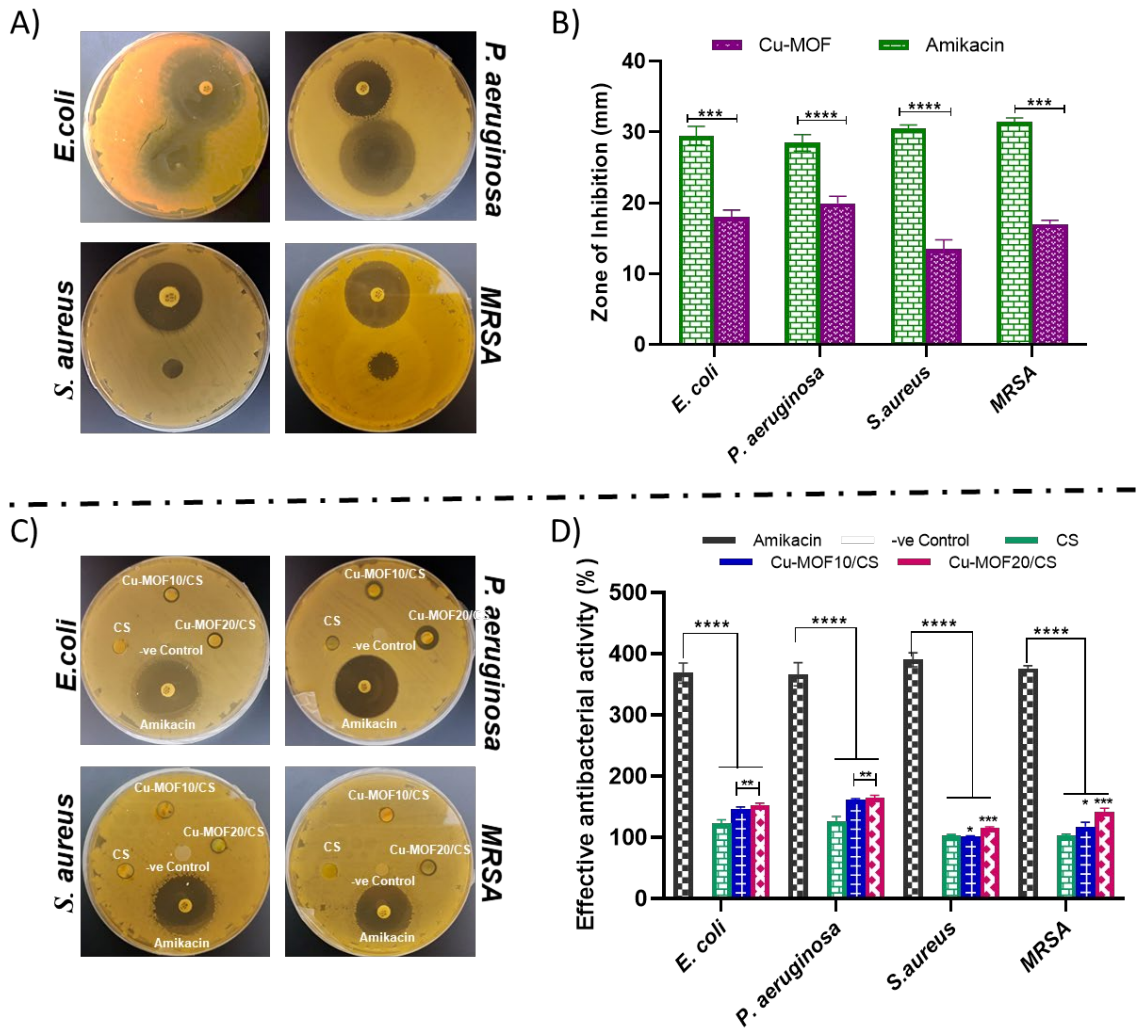


**Figure 4:** *In vitro* antibacterial activity Cu-MOF & synthesized membranes (CS, Cu-MOF10/CS, and Cu-MOF20/CS). against *E. coli*, *Pseudomonas aeruginosa*, *S. aureus*, *MRSA*; A) Digital Photographs of plates showing the zone of inhibition of Cu-MOF against *E. coli*, *Pseudomonas aeruginosa*, *S. aureus* & *MRSA*; B) Statistical Graph representing the zone of inhibition of Cu-MOF against *E. coli*, *Pseudomonas aeruginosa*, *S. aureus*, *MRSA*. Results are presented as n=3+SD; \*\*\*\*P≤0.0001 denotes +ve Control (Amikacin) versus Cu-MOF); C) Digital Photographs of plates showing the zone of inhibition of synthesized membranes against *E. coli*, *Pseudomonas aeruginosa*, *S. aureus* & *MRSA*; Statistical Graph representing the effective antibacterial activity of synthesized membranes (CS, Cu-MOF10/CS, and Cu-MOF20/CS), against *E. coli*, *Pseudomonas aeruginosa*, *S. aureus*, *MRSA*. Results are presented as n=3+SD; \*\*\*\*P≤0.0001 denotes Cu-MOF10/CS, and Cu-MOF20/CS).

### **3.11 CAM assay**

Figure 5(A) displays the qualitative outcomes of neovascularization stimulated by CS, Cu-MOF10/CS, and Cu-MOF20/CS. Using digital photos, AngioQuant software was used to determine the fold change in blood vessels length, size, and junctions from the pre-existing ones. Figure 5(C, D and E) displays the histograms of these blood vessel features. The total number of blood vessels surrounding the membranes was determined using Image J.

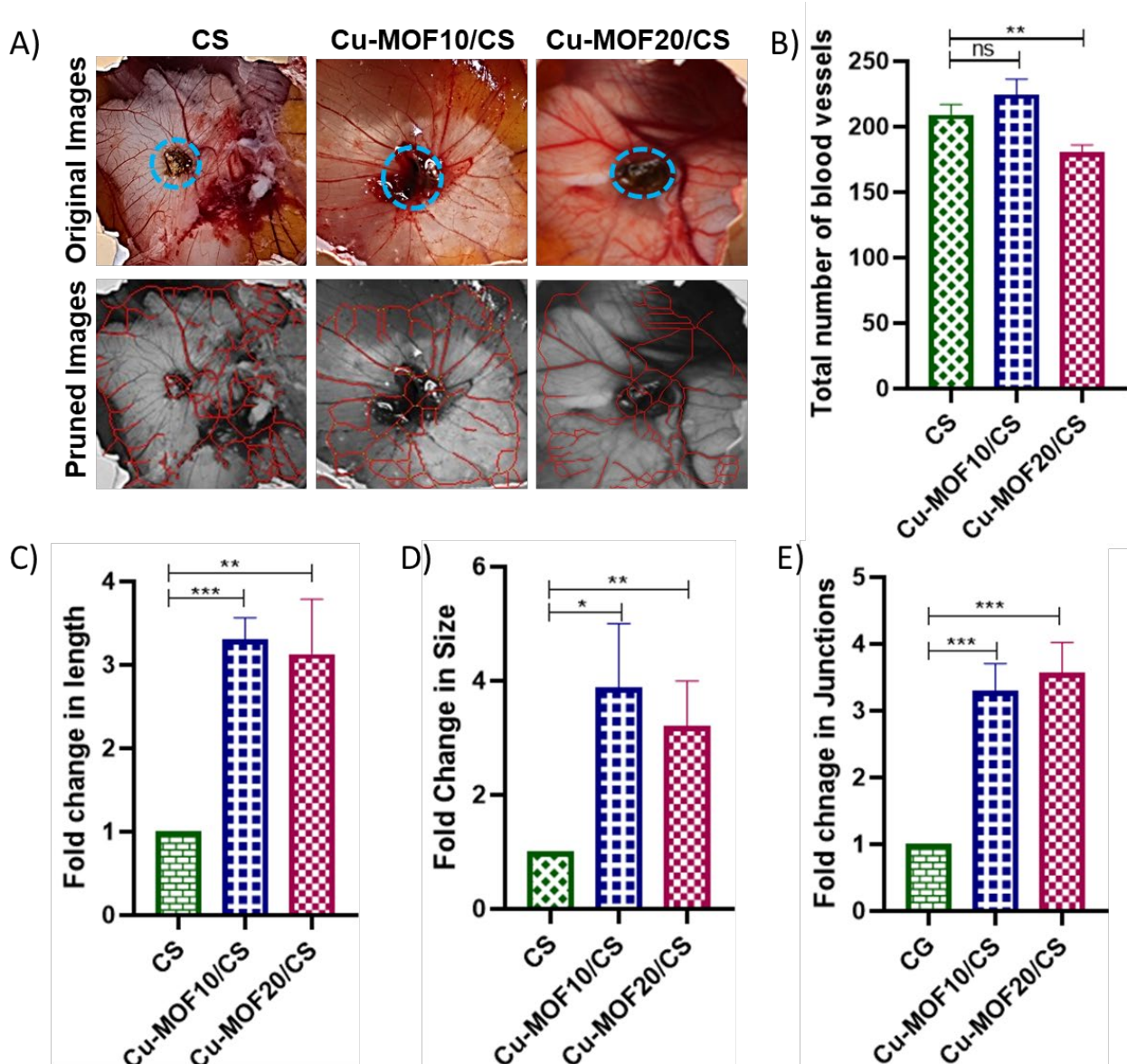


**Figure 5:** *In ovo* angiogenesis assay performed using chick embryo model; A) Qualitative images of a chick embryo model after 7 days incubation with CS, Cu-MOF10/CS, and Cu-MOF20/CS; B) Quantification of angiogenic potential via imageJ software ( $***P < 0.001$  denotes CS versus Cu-MOF20/CS & ns  $p > 0.05$ ); AngioQuant software analysis for Angiogenic variables such as, C) blood vessel length ( $***P < 0.001$  denotes CS versus Cu-MOF10/CS &  $**P < 0.01$  denotes CS versus Cu-MOF20/CS), D) size ( $***P < 0.001$  denotes CS versus Cu-MOF20/CS & ns  $p > 0.05$ ); and E) junctions (branches) ( $*P < 0.1$  denotes CS versus Cu-MOF10/CS &  $**P < 0.01$  denotes CS versus Cu-MOF20/CS).

On day 14 of CAM, angiogenic effects of CS, Cu-MOF10/CS and Cu-MOF20/CS membranes on chorioallantoic membrane of chick are shown in Fig 5(A & B). In comparison to CS, there was dense and visible network of blood vessels surrounding the Cu-MOF10/CS. By using Image J software, almost 244 number of blood vessels around Cu-MOF10/CS than CS (202) and Cu-MOF20/CS (186) have been observed. The histogram displayed in Figure 5(C-E) represents the fold change in length, size and junctions of newly formed blood vessels. Cu-MOF10/CS showed almost 4 folds increase in size and 3 folds increase in length and junctions of blood vessels compared to CS and Cu-MOF20/CS. So, Cu-MOF10/CS showed the better angiogenic potential among all three membranes.

### **3.12 *In vivo* infectious wound healing effect of Cu-MOF**

The phases of healing that overlap are hemostasis, re-epithelialization, proliferation, inflammation, and remodeling. A critical step in the transition from the inflammatory to the repair stages is the clumping and activation of inflammatory cells. To forecast the pace of wound healing, we recorded overall wound closure results. Figure 6 (B) displays the general wound closure images for each of the four groups at different time intervals.

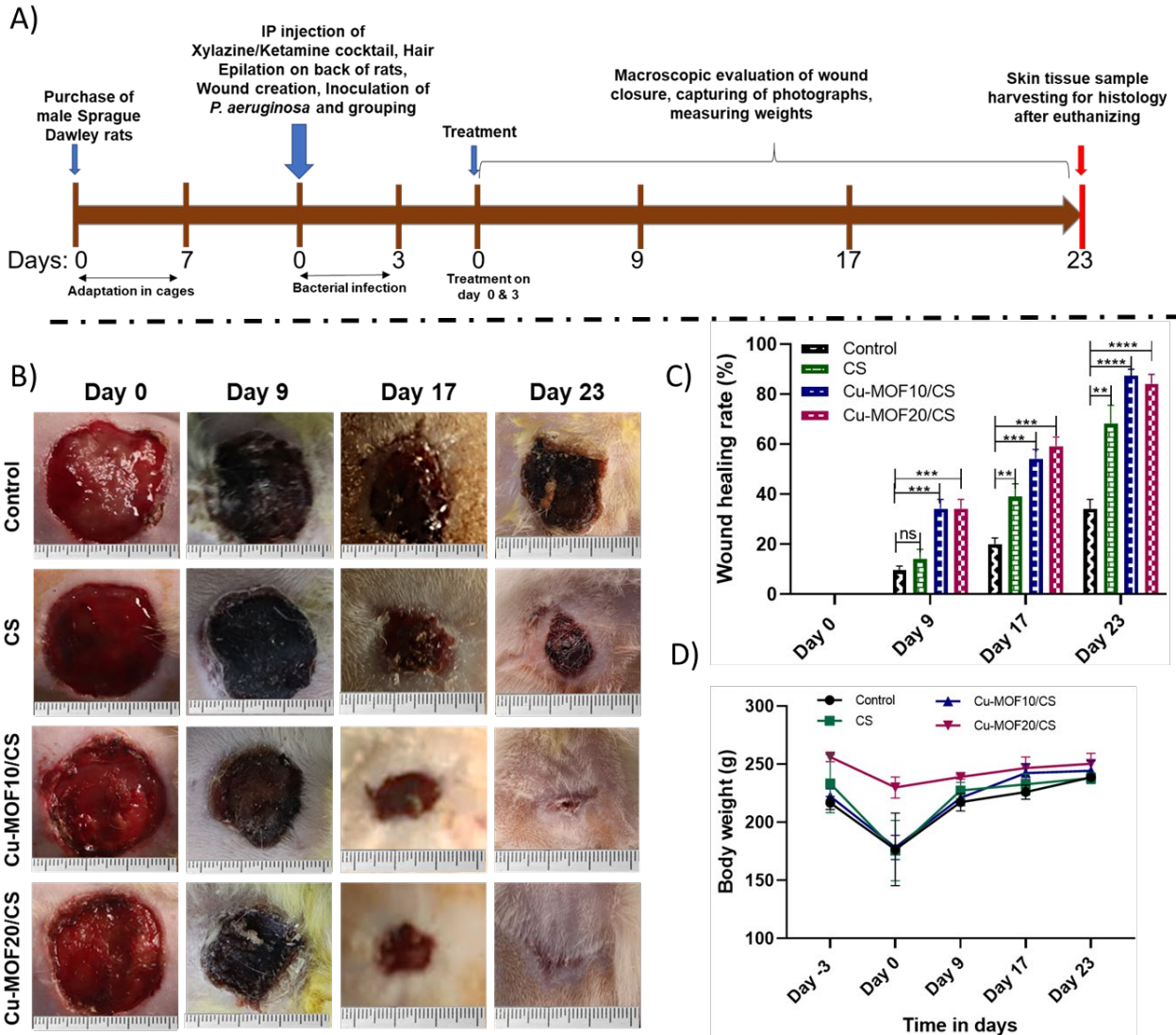


**Figure 6:** A) Schematic diagram for *in vivo* experiment; Effects of CS, Cu-MOF10/CS & Cu-MOF20/CS on wound healing in vivo, B) Comparison of wound healing in Control, CS, Cu-MOF10/CS & Cu-MOF20/CS at different time intervals (Days 0, 9, 17 and 23); C) Quantitative analysis of wound closure rates (Results are presented as mean  $\pm$  SD,  $n=4$ . \*\* $P<0.01$ , \*\*\* $P<0.001$ , \*\*\*\* $P<0.0001$  ns  $P\geq 0.05$ ); D) Comparison of rat's body weight after treatment with Control, CS, Cu-MOF10/CS & Cu-MOF20/CS at Day 0, 9 17 and 23.

To investigate the healing capability and process of Cu-MOF-10 on full thickness surgical wounds, a full-thickness excision wound model in Sprague-Dwaley rats was used. The results of Figure 6

(B) showed that, as compared to the control and CS, the Cu-MOF-20 and Cu-MOF-10 treated group had a comparatively greater degree of wound closure on 9<sup>th</sup>, 17<sup>th</sup> and 23<sup>rd</sup> days of treatment. Overall, on day 23, almost all the wounds in the Cu-MOF-20 and Cu-MOF-10 were almost completely closed, while the lesions in the control group and CS groups were still macroscopically open. The healing rate of the Cu-MOF-10 group rose dramatically from day 9 to day 23 (Figure 6 (C), from 34.33% to 87.67%, similarly the Cu-MOF-20 group rose from 34.33% to 84.5%, whereas the CS group rose slowly from 11% to 63.5%. On day 23<sup>rd</sup>, there was a significant difference in the wound healing rate between the Cu-MOF-10 and the Cu-MOF-20 groups and Control. The animals were weighed both prior to and throughout the course of the treatments. In three days after injection, rats in all groups lost weight, however over the 23<sup>rd</sup> days of study all of the animals gain weight which was close to their initial weights.

On day 0 and 23, from the infected wounds, a small number of bacterial colonies were counted on the agar plates via colony forming Unit (CFU assay, in the all groups (Control, CS, Cu-MOF10/CS, and Cu-MOF20/CS) by using spread plate method (SPM) (42) On day 0, more colonies in a range of  $9-10 \times 10^4$  CFU/ml were observed in all cases. As shown in figure 7(A & B), after treatment on day 23<sup>rd</sup> the bacterial survival rates in Cu-MOF20/CS was about approximately less than 1%, while around 3% of the bacteria survived in in Cu-MOF10/CS group nanoparticles. These differences could be attributed to the anti-bacterial activity of Cu-MOF. These results confirmed that Cu-MOF20/CS possessed good level of antibacterial performance in infected wounds in rats.

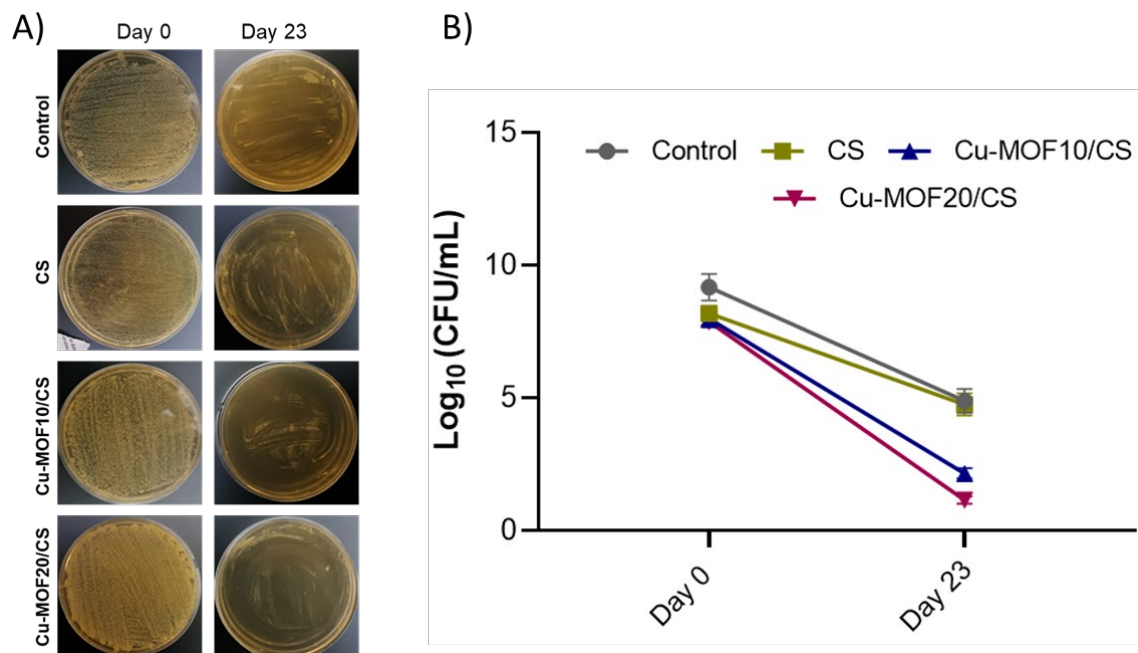


**Figure 7:** A) Agar plates- swabs of *P. aeruginosa* from the rat wounds of groups (Control, CS, Cu-MOF10/CS & Cu-MOF20/CS) on day 0 and 23; B) Colony-forming units (CFU) count of bacterial from groups (Control, CS, Cu-MOF10/CS & Cu-MOF20/CS) using spread plate method (SPM).

### 3.13 Histological analysis of infectious wound tissues

The renewed skin tissues from the four groups were removed and histologically assessed after the rats were euthanized on day 23. Through H&E staining, it was observed that, on day 23, wound sites in both MOF groups had higher number of neovascular endothelial cells than in CS and control groups, as shown in Figure 8. In addition, Cu-MOF-10 group showed minimal inflammatory cells. The control group displayed dermal cell necrosis, a strong inflammatory response, and a deficiency of neovascular endothelial cells. On 23<sup>rd</sup> day, dermal layer in control group was notably thinner, and inflammatory cells predominated in the granulation tissue. Analysis of H&E-stained tissue sections revealed that the defect wounds treated with Cu-MOF-10

group had comparatively more regenerated blood vessels, re-epithelization and nearly full dermal tissue regeneration under a uniform and complete layer of epidermis. Overall, control, CS and Cu-MOF-20 groups did not fully re-epithelialize, and much less hair follicles were detected in the dermal tissues of Cu-MOF-20 and CS groups and not any in control group. The Cu-MOF-10 group has effectively accelerated wound healing by lowering inflammation, promoting angiogenesis and granulation at the wound sites, leading to tissue regeneration, and remodeling of the physiological structures. Thus, Cu-MOF-10 represent a potential class of biomaterials for the treatment of significant wound healing.

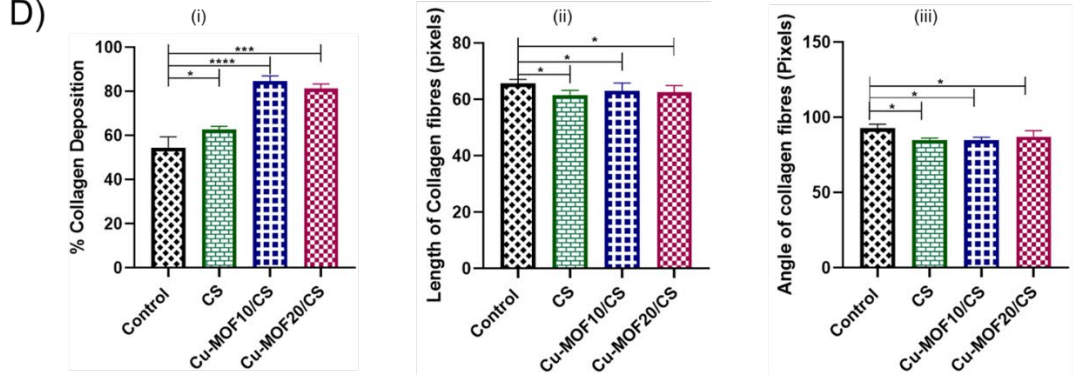
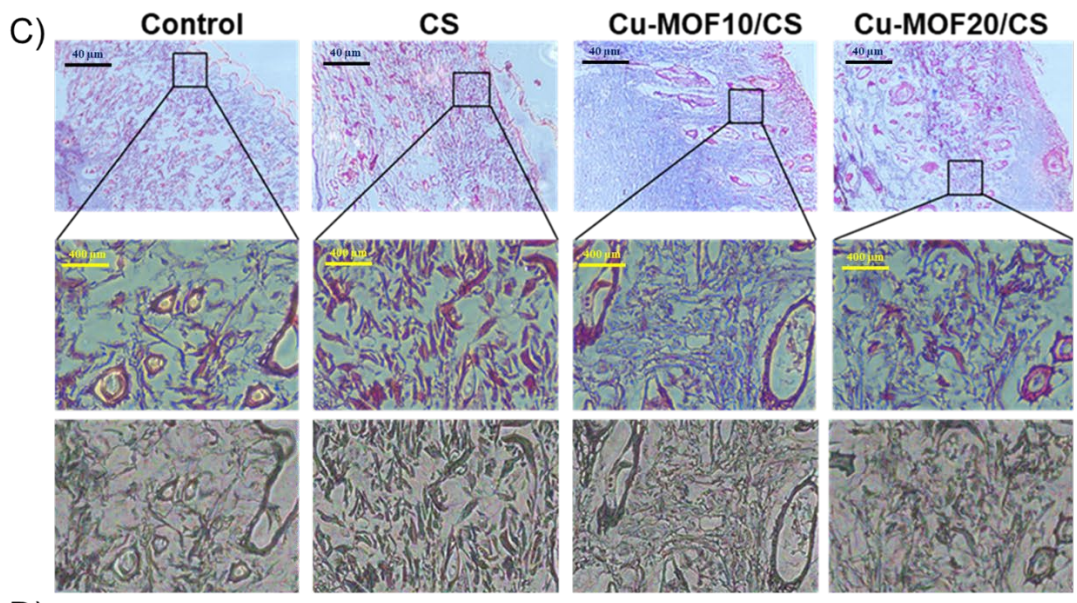
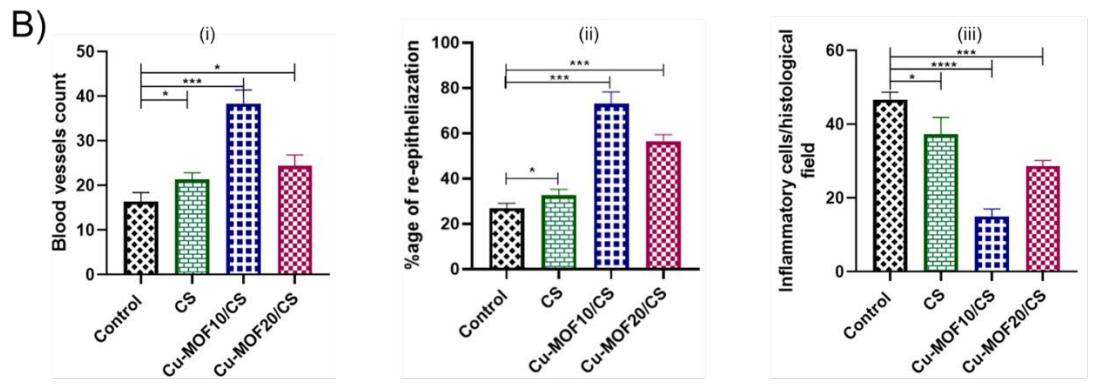
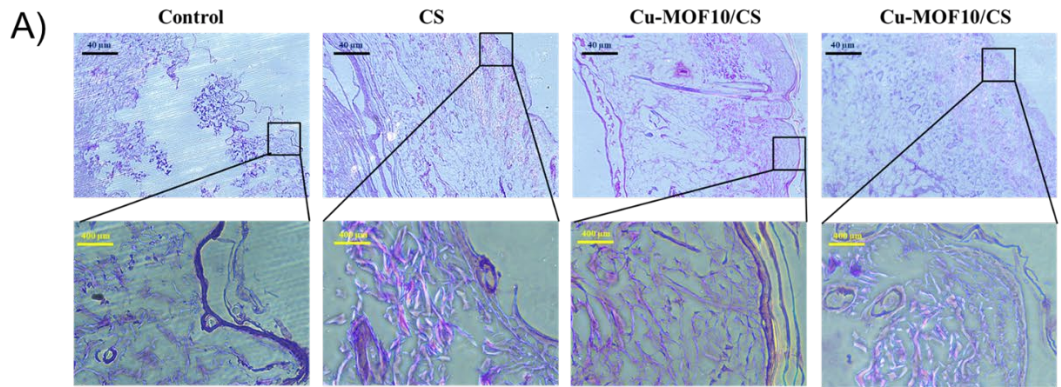


**Figure 8:** On the 23<sup>rd</sup> day of treatment with Control, CS, Cu-MOF10/CS & Cu-MOF20/CS, A) H&E-stained histological analysis of healed wound skin showing epithelium formation blood vessels & inflammatory cells /histological field; B) (i) Quantification of blood vessel; (ii) %age re-epithelization. (iii) Inflammatory cells per field of view via H&E-stained histological analysis; C) Masson trichrome staining of healed wound skin showing collagen fibres (% collagen deposition): D(i)% Collagen deposition; (ii) Length and (iii) angle of collagen fibers per histological analysis (Results are presented as n=5+SD; \*\*\*\* $P \leq 0.0001$ , \* $P \leq 0.1$ , \*\*\* $P \leq 0.001$ ).

### 3.14 Analysis of Collagen deposition, length, and angle

Collagen is very essential in wound healing process. Fibroblasts in the dermal layer produce collagen, which is the primary component of extracellular matrix. The procedure of wound healing depends on the deposition of collagen because it creates three-dimensional framework needed to encourage cell relocation, variation, and propagation. In this study, collagen deposition, length and angle were evaluated using Masson's trichrome staining, highlighting collagen in blue. In figure 8(B), on day 23, there was a noticeably higher amount of collagen deposition in the Cu-MOF-10 group than in the other treatment groups. The deviation in collagen fiber angles and length between control and treated groups were measured through CT-FIRE software, indicates definite distinctions in collagen makeup and trait, represented in figure 8 (D) (ii). Collagen fiber lengths were found to be greater in the control group and lower in the other treatment groups, except for the CS group, which had shorter collagen fibers. This suggests that the treatment groups had more collagens than the control group. Moreover, the angle of collagen fibers acts a fundamental role in determining their property and compaction in figure 8 (D) (iii). A larger angle in the control group suggests less organized and compacted collagen fibers, while smaller angles in the treated groups indicate a more structured and tightly packed arrangement. This difference highlights the prospective effect of treatments on improving collagen fiber alignment and quality, contributing

to improved wound healing and tissue reform in the treated groups. These findings demonstrated that the Cu-MOF-10 might accelerate wound healing and tissue remodeling by encouraging more vigorous collagen deposition.

#### **4. Discussion**

In addition to posing serious health risks, wounds place a heavy financial strain on healthcare systems around the world. Due to a number of problems, typical wound healing techniques now in use are no longer successful for infected wounds. Due to resistant of bacteria against anti-bacterial drugs, alternate approaches that are safe, efficient, and promote early wound healing are being investigated by researchers (43). Acute and chronic wounds heal more slowly and become compromised when healing process is protracted, deprived, or disordered (44). Infection control and neovascularization are two of the most significant aspects in normal physiological healing of wounds. When these factors are negotiated or disturbed, it can substantially inhibit the healing process and precedent to complications.

MOFs are highly tunable hybrid materials and recently garnered more scientific attention for their potential to effectively heal chronic wounds due to their anti-bacterial and angiogenic activities. MOFs can address problems of wound healing by promoting faster and safer wound healing (45). In current study, Cu-MOF was prepared by sonochemical method. The porous scaffold based on copper MOF loaded into chitosan was successfully synthesized via a practical two-step synthetic route, in first step homogenous mixture of chitosan and Cu-MOF was obtained and in second step the solution was lyophilized using freeze dryer. The highly porous membranes are suitable to support proliferation of cells. The materials were employed for physiochemical characterization, including FTIR, SEM, and swelling studies. SEM analysis confirmed the high porosity, which was increased with the increase in concentration of Cu-MOF. The decrease in swelling ratio in Cu-

MOF20/CS dressing was observed which could be due to the formation of more compact structure after adding MOF, higher amount of the MOF, the more harder resulting materials are expected (46).

One of the fundamental need for clinical dressings is good biocompatibility (32). The biocompatibility of membranes is commonly assessed by two main methods: cytocompatibility (cell viability) and hemocompatibility assays (32). The cytocompatibility of dressings may harm or even kill normal cells, which would impair viability of the cells. Thus, non-cytotoxic activity is an important characteristic of any ideal wound dressing prior to human use (47). Materials are considered non-toxic if cell viability is >75% according to ISO 10993-5:2009 (48). In present study, the Cu-MOF/CS showed viability of fibroblast cells more than 100%, that is also in accordance with the results reported by Wang and co-workers [(48)].

All the tested materials showed good hemocompatibility, the values were below 5% which are in accordance with international standards (49). Blood clotting indexes of CS, Cu-MOF10/CS and Cu-MOF20/CS (2.78, 1.3 and 0.9%) were much lower than that of positive control (19.8%), suggesting that these quickly absorbed blood, enhanced blood viscosity and encouraged aggregation of red blood cells and platelets. This is mostly due to robust electrostatic interaction between +vely charged chitosan and -vely charged nucleophilic cells in blood (50) that lead initial adsorption of plasma proteins on chitosan, followed by adhesion and activation of platelets that lead to the formation of clot. These results are in congruent with literature where blood clotting index of polyurethane and chitosan loaded with metal organic frameworks was 19.67% and with nanoparticles 24.98% , these are >5%, and much more than the recommended ISO standard (51, 52).

One of the primary reasons why chronically infected wounds take longer to heal is excessive oxidative stress (53). Consequently, the hydrogel or dressings capable of scavenging reactive oxygen species (ROS) have emerged as a viable approach to management of infected wounds (54). Numerous studies have demonstrated that antioxidant dressings may efficiently eliminate reactive oxygen species (ROS) from wound surface and accelerate wound healing (54, 55). Radical scavenging activity of various metal organic frameworks have been reported in literature, i.e, copper-based metal–organic framework (Cu MOF) nanozyme (56) and cerium based metal organic framework into cellulose sheet (57) have been found to be antioxidant. The antioxidant potential of the Cu-MOF loaded membranes was tested against free radicals by using DPPH assay. Among three synthesized membranes, Cu-MOF20/CS dressing showed maximum 83% scavenging potential, which highlights its role in regulating inflammatory responses, and aiding wound healing.

A key component of effective wound healing is shielding wounds from infections that impede healing process (7). The microbes cause infections at wound site and are extensively dispersed throughout the environment. It is commonly recognized that chitosan has antibacterial properties against bacteria. These might be due to interactions between negatively charged moieties on bacterial cell membrane and cationic structure of chitosan, which cause bacteria to burst and die (58). Cu-MOF loaded chitosan membranes are effective against all four bacteria due to their ability to inactivate their metabolic machinery, resist bacterial cell acidity, scavenge reactive oxygen species, and maintain their bactericidal capacity by altering the signal transduction pathway (59).

The obtained antibacterial property of Cu-MOF/CS can be attributed to Cu-MOF's ability to degrade the cell membranes (60). The interaction of copper with the cysteine–thiol group (in bacterial cell membrane) is believed to be the antibacterial mechanism (61). Copper ions can

combine with thiol groups to generate S–Cu complexes, which impede the afflicted proteases' normal enzymatic action. The released active cations attach onto the surface of the bacterial cell membrane through endocytosis and leads to bacterial death (62).

Exopolysaccharides (EPSs) secreted by bacterial cells and activated by environmental signals stimulate bacteria to form biofilms. Therefore, if EPS generation can be inhibited, biofilm formation will be restricted (63). Conjugating metal organic framework with polymers has been studied recently by Rajamohan et. al., in an effort to prevent the formation of biofilm (64). Our results in this paper indicate that Cu-MOF10/CS shows an enhanced anti-biofilm effect, with 63 and 43% inhibition of *P. aeruginosa* and *MRSA* biofilm respectively within 24 hours. The process of growth of new blood vessels from pre-existing ones is known as angiogenesis. It helps new blood vessels growth and formation of granulation tissues which are essential for wound healing (65). We tested the angiogenic activity of the synthesized dressings by using chorioallantoic membrane assay, our results showed that Cu-MOF10/CS stimulated neovascularization (length, size and junctions of blood vessels) by 3-4 folds better than CS and Cu-MOF20/CS. It is the 1<sup>st</sup> report where angiogenic potential of copper metal organic framework loaded chitosan (Cu-MOF/CS) membranes by CAM assay has been investigated.

To study the effect of prepared Cu-MOF dressings on full thickness wound healing, Sprague-Dwaley rats were given full-thickness surgical excision wounds. These wounds were treated with Cu-MOF/CS, and the impact on healing was monitored. In comparison to wounds treated with CS or sham treatment (control), Cu-MOF-10 treated wounds exhibited less inflammatory cells, significantly higher collagen deposition, reasonable fiber length and angle, stimulated angiogenesis, and wounds were healed faster. In comparison to Cu-MOF-10 treated group, Cu-MOF-20 treated wound showed a considerable reduction in inflammatory cells, good collagen

deposition, improved fiber length and angle, satisfactory wound healing, and comparatively low angiogenesis. Cu-MOF-10 dramatically enhanced angiogenesis and collagen deposition, as evidenced by histology of the repaired areas. These results highlight Cu-MOF-10's significant potential to accelerate wound healing by affecting cellular comebacks and tissue regeneration (36).

The common risk factor for delayed wound healing is bacterial infection. An increasing number of research studies have indicated that as part of wound management a special attention should be given to infection control. (66). So, based on *in vitro* tests (sufficient exudate uptake capacity, ability to provide suitable microenvironment for cell proliferation, excellent free radical scavenging, antibacterial and antibiofilm and angiogenic potential) and *in vivo* studies in infected wound rat model, Cu-MOF 10/CS is suggested to treat diabetic and chronic infected wounds.

Overall, antibacterial metal ions (copper) inhibit the growth of bacteria and has potential to replace the antibiotics and other drugs that have harmful side effects such as producing bacteria resistant strains. Regarding demerit, the copper-MOF will need further detailed biological investigations *in vitro* and *in vivo* before could be used on humans. MOF-based materials may have the potential to be effective antimicrobial agents against infectious diseases, curbing antibiotic resistance, but detailed studies are needed to validate it.

## 5. Conclusion

In summary, the manufacturing of multifunctional porous Cu-MOF loaded chitosan membranes has been achieved by freeze drying. The antibacterial activity of the Cu-MOF materials showed that these were effective against Gram-negative bacteria (*E. coli* and *P. aeruginosa*) and Gram-positive bacteria (*S. aureus* and *MRSA*) with zone of inhibitions 13, 14, 9 and 11mm respectively. After loading of Cu-MOFs into the chitosan membranes, Cu-MOF20/CS showed effective

antibacterial activity against the tested strains; *E. coli* (149.2%), *P. aeruginosa* (165%) *S. aureus* (117.8%) and *MRSA* (142%). Similarly, Cu-MOF10/CS and Cu-MOF20/CS were able to eradicate biofilms effectively and it was also found that Cu-MOF20/CS showed higher activity against *P. aeruginosa*. The prepared membranes (Cu-MOF20/CS) also showed 83% ROS scavenging ability and, in CAM assay, Cu-MOF10/CS stimulated angiogenesis comparatively better than Cu-MOF/20 and CS. *In vivo* experiment demonstrated that Cu-MOF10/CS significantly promoted healing of *P. aeruginosa*-infected full-thickness wounds in rats over 23 days. Overall, as desired, Cu-MOF loaded dressings were able to control infection in wounds and stimulated angiogenesis, which resulted in the faster wound healing in rats. These multifunctional features of the synthesized dressings provide a great opportunity in the treatment of complicated wounds such as infected non-healing wounds and chronic foot diabetic ulcers.

#### **Acknowledgement:**

We would like to acknowledge Higher Education Commission (HEC) Pakistan for financial support under HEC Pakistan and British Council UK for providing funding support under ICRG project number 20-ICRG-33/RGM/HEC/2020 and Pakistan Science Foundation for providing funds under PSF-Tubitak Project Number PSF/TUBITAK III/Biomed/C/COMSATS (19).

#### **References**

[1] Jackson TA, Neo YP, Sisinthy SP, Gorain B. Delivery of therapeutics from layer-by-layer electrospun nanofiber matrix for wound healing: An update. *J Pharm Sci.* 2021;110(2):635-53. doi.org/10.1016/j.xphs.2020.10.003

[2] Ghomi ER, Lakshminarayanan R, Chellappan V, Verma NK, Chinnappan A, Neisiany RE, Amuthavalli K, Poh ZS, Wong BH, Dubey N, Narayan R. Electrospun aligned PCL/gelatin scaffolds mimicking the skin ECM for effective antimicrobial wound dressings. *Adv Fiber Mater.* 2023;5(1):235-51. doi.org/10.1007/s42765-022-00216-w

- [3] Li ChengHsuan LC, Chen XinHong CX, Landis RF, Geng YingYing GY, Makabenta JM, Lemnios W, Akash Gupta AG, Rotello VM. Phytochemical-based nanocomposites for the treatment of bacterial biofilms. *ACS infectious diseases*. 2019;5(9):1590-6. doi.org/10.1021/acsinfecdis.9b00134
- [4] Zeng Y, Wang C, Lei K, Xiao C, Jiang X, Zhang W, Wu L, Huang J, Li W. Multifunctional MOF-Based Microneedle Patch With Synergistic Chemo-Photodynamic Antibacterial Effect and Sustained Release of Growth Factor for Chronic Wound Healing. *Adv Healthcare Mater*. 2023:2300250. doi.org/10.1002/adhm.202300250
- [5] Huang F, Cai X, Hou X, Zhang Y, Liu J, Yang L, Liu Y, Liu J. A dynamic covalent polymeric antimicrobial for conquering drug-resistant bacterial infection. *Exploration*; 2022: Wiley Online Library. doi.org/10.1002/EXP.20210145
- [6] Shi C, Wang C, Liu H, Li Q, Li R, Zhang Y, Liu Y, Shao Y, Wang J. Selection of appropriate wound dressing for various wounds. *Front Bioeng Biotechnol*. 2020;8:182. doi.org/10.3389/fbioe.2020.00182
- [7] Huang Y, Mu L, Zhao X, Han Y, Guo B. Bacterial growth-induced tobramycin smart release self-healing hydrogel for *Pseudomonas aeruginosa*-infected burn wound healing. *ACS nano*. 2022;16(8):13022-36. doi.org/10.1021/acsnano.2c05557
- [8] Lai-Cheong JE, McGrath JA. Structure and function of skin, hair and nails. *Medicine*. 2013;41(6):317-20. doi.org/10.1016/j.mpmed.2013.04.017
- [9] Zhou F, Sun S, Cui C, Li X, Wu S, Ma J, Chen S, Li CM. Zinc ions and ciprofloxacin-encapsulated chitosan/poly ( $\epsilon$ -caprolactone) composite nanofibers promote wound healing via enhanced antibacterial and immunomodulatory. *Int J Biol Macromol*. 2023;253:127086. doi.org/10.1016/j.ijbiomac.2023.127086
- [10] Zhang C, Yang X, Yu L, Chen X, Zhang J, Zhang S, Wu S. Electrospun polyasparthydrazide nanofibrous hydrogel loading with in-situ synthesized silver nanoparticles for full-thickness skin wound healing application. *Mater Design*. 2024:112818. doi.org/10.1016/j.matdes.2024.112818
- [11] Li Y, Zhao W, Chen S, Zhai H, Wu S. Bioactive electrospun nanoyarn-constructed textile dressing patches delivering Chinese herbal compound for accelerated diabetic wound healing. *Mater Design*. 2024;237:112623. doi.org/10.1016/j.matdes.2023.112623

- [12] Shahraki S, Delarami HS, Khosravi F, Nejat R. Improving the adsorption potential of chitosan for heavy metal ions using aromatic ring-rich derivatives. *J Colloid Interface Sci.* 2020;576:79-89. doi.org/10.1016/j.jcis.2020.05.006
- [13] Croisier F, Jérôme C. Chitosan-based biomaterials for tissue engineering. *Euro Polym J.* 2013;49(4):780-92. doi.org/10.1016/j.eurpolymj.2012.12.009
- [14] Rahnamaee SY, Seyedkhani SA, Saed AE, Sadrnezhad SK, Seza A. Bioinspired TiO<sub>2</sub>/chitosan/HA coatings on Ti surfaces: biomedical improvement by intermediate hierarchical films. *Biomed Mater.* 2022;17(3):035007. doi.org/article/10.1088/1748-605X/ac61fc/meta
- [15] Shivakumar P, Gupta MS, Jayakumar R, Gowda DV. Prospection of chitosan and its derivatives in wound healing: Proof of patent analysis (2010–2020). *Int J Biol Macromol.* 2021;184:701-12. doi.org/10.1016/j.ijbiomac.2021.06.086
- [16] Miguel SP, Moreira AF, Correia IJ. Chitosan based-asymmetric membranes for wound healing: A review. *Int J Biol Macromol.* 2019;127:460-75. doi.org/10.1016/j.ijbiomac.2019.01.072
- [17] Gao D, Mi Y, Gao Z. doi.org/10.1016/j.matlet.2020.128237. *Mater Lett.* 2020;276:128237.
- [18] Ahmadijokani F, Molavi H, Rezakazemi M, Tajahmadi S, Bahi A, Ko F, Aminabhavi TM, Li JR, Arjmand M. UiO-66 metal–organic frameworks in water treatment: A critical review. *Prog Mater Sci.* 2022;125:100904. doi.org/10.1016/j.pmatsci.2021.100904
- [19] Ahmadijokani F, Molavi H, Rezakazemi M, Aminabhavi TM, Arjmand M. Simultaneous detection and removal of fluoride from water using smart metal-organic framework-based adsorbents. *Coord Chem Rev.* 2021;445:214037. doi.org/10.1016/j.ccr.2021.214037
- [20] Barjasteh M, Vossoughi M, Bagherzadeh M, Bagheri KP. Green synthesis of PEG-coated MIL-100 (Fe) for controlled release of dacarbazine and its anticancer potential against human melanoma cells. *Int J Pharm.* 2022;618:121647. doi.org/10.1016/j.ijpharm.2022.121647
- [21] Molavi H, Shojaei A. Mixed-matrix composite membranes based on UiO-66-derived MOFs for CO<sub>2</sub> separation. *ACS Appl Mater Interfaces.* 2019;11(9):9448-61. doi.org/10.1021/acsami.8b20869
- [22] Barjasteh M, Vossoughi M, Bagherzadeh M, Bagheri KP. doi.org/10.1016/j.cej.2022.138987 *Chem Eng J.* 2023;452:138987.

- [23] Zhu Y, Zhang Z, Li W, Lei Z, Cheng N, Tan Y, Mu S, Sun X. Highly exposed active sites of defect-enriched derived MOFs for enhanced oxygen reduction reaction. *ACS Sustain Chem Eng.* 2019;7(21):17855-62. doi.org/10.1021/acssuschemeng.9b04380
- [24] Dhakshinamoorthy A, Navalón S, Asiri AM, Garcia H. Gold-nanoparticle-decorated metal-organic frameworks for anticancer therapy. *Chem Med Chem.* 2020;15(23):2236-56. doi.org/10.1002/cmdc.202000562
- [25] Deng Q, Sun P, Zhang L, Liu Z, Wang H, Ren J, Qu X. Porphyrin MOF dots-based, function-adaptive nanoplatform for enhanced penetration and photodynamic eradication of bacterial biofilms. *Adv Funct Mater.* 2019;29(30):1903018. doi.org/10.1002/adfm.201903018
- [26] Wang Z, Hu S, Yang J, Liang A, Li Y, Zhuang Q, Gu J. Nanoscale zr-based MOFs with tailorable size and introduced mesopore for protein delivery. *Adv Funct Mater.* 2018;28(16):1707356. doi.org/10.1002/adfm.201707356
- [27] Yang M, Zhang J, Wei Y, Zhang J, Tao C. Recent advances in metal-organic framework-based materials for anti-staphylococcus aureus infection. *Nano Res.* 2022;15(7):6220-42. doi.org/10.1007/s12274-022-4302-x
- [28] Yuan Y, Wu H, Lu H, Zheng Y, Ying JY, Zhang Y. ZIF nano-dagger coated gauze for antibiotic-free wound dressing. *Chem Commun.* 2019;55(5):699-702. doi.org/10.1039/C8CC08568D
- [29] Huang G, Xu D, Qin Z, Liang Q, Xu C, Lin B. Universal, controllable, large-scale and facile fabrication of nano-MOFs tightly-bonded on flexible substrate. *Chem Eng J.* 2020;395:125181. doi.org/10.1016/j.cej.2020.125181
- [30] Yao X, Zhu G, Zhu P, Ma J, Chen W, Liu Z, Kong T. Omniphobic ZIF-8@ Hydrogel membrane by microfluidic-emulsion-templating method for wound healing. *Adv Funct Mater.* 2020;30(13):1909389. doi.org/10.1002/adfm.201909389
- [31] Abbasi AR, Akhbari K, Morsali A. Dense coating of surface mounted CuBTC metal-organic framework nanostructures on silk fibers, prepared by layer-by-layer method under ultrasound irradiation with antibacterial activity. *Ultrasonics sonochemistry.* 2012;19(4):846-52.
- [32] Saghebasl S, Amini H, Nobakht A, Haiaty S, Bagheri HS, Hasanpour P, Milani M, Saghati S, Naturi O, Farhadi M, Rahbarghazi R. Polyurethane-based nanofibrous mat containing porphyrin with photosensitivity

and bactericidal properties can promote cutaneous tissue healing in rats. *J Nanobiotechnol.* 2023;21(1):313. doi.org/10.1186/s12951-023-02082-z

[33] Barjasteh M, Dehnavi SM, Seyedkhani SA, Rahnamaee SY, Golizadeh M. Improved biological activities of dual nanofibrous chitosan/bacterial cellulose wound dressing by a novel silver-based metal-organic framework. *Surf Interfaces.* 2023;36:102631. doi.org/10.1016/j.surfin.2023.102631

[34] Ramzan A, Mehmood A, Ashfaq R, Andleeb A, Butt H, Zulfiqar S, Nasir M, Hasan A, Khalid K, Yar M, Malik K. Zinc oxide loaded chitosan-elastin-sodium alginate nanocomposite gel using freeze gelation for enhanced adipose stem cell proliferation and antibacterial properties. *Int J Biol Macromol.* 2023;233:123519. doi.org/10.1016/j.ijbiomac.2023.123519

[35] Rafi R, Zulfiqar S, Asad M, Zeeshan R, Zehra M, Khalid H, Akhtar N, Yar M. Smart wound dressings based on carbon doped copper nanoparticles for selective bacterial detection and eradication for efficient wound healing application. *Mater Today Commun.* 2023;35:105914. doi.org/10.1016/j.mtcomm.2023.105914

[36] Abid S, Zulfiqar S, Anjum MA, Bullock AJ, MacNeil S, Yar M. An alginate-Based tube gel delivering 2-deoxy-D-ribose for stimulation of wound healing. *J Biomater Appl.* 2023;38(2):264-79. doi/abs/10.1177/08853282231191218

[37] Zehra M, Zubairi W, Hasan A, Butt H, Ramzan A, Azam M, Mehmood A, Falahati M, Chaudhry AA, Rehman IU, Yar M. Oxygen generating polymeric nano fibers that stimulate angiogenesis and show efficient wound healing in a diabetic wound model. *Int J Nanomedicine.* 2020:3511-22. doi/full/10.2147/IJN.S248911

[38] Sharif S, Sahin O, Khan IU, Büyükgüngör O. 1-D and 2-D coordination polymers of cerium (III) with pyridine-2, 4, 6-tricarboxylic acid: synthesis and structural, spectroscopic, and thermal properties. *J Coord Chem.* 2012;65(11):1892-904. doi.org/10.1080/00958972.2012.685165

[39] Lee JY, Choi J-H. Copper-based metal-organic framework for highly efficient adsorption of lead ions from aqueous solution. *Mater Res Express.* 2022;9(9):095505. DOI 10.1088/2053-1591/ac93ea

[40] Mirhosseini H, Shamspur T, Mostafavi A, Sargazi G. A novel ultrasonic assisted-reverse micelle procedure to synthesize Eu-MOF nanostructure with high sono/sonophotocatalytic activity: a systematic

study for brilliant green dye removal. *J Mater Sci: Mater Electr.* 2021;32(18):22840N-59. doi.org/10.1007/s10854-021-06762-0

[41] Khan A, Andleeb A, Azam M, Tehseen S, Mehmood A, Yar M. Aloe vera and ofloxacin incorporated chitosan hydrogels show antibacterial activity, stimulate angiogenesis and accelerate wound healing in full thickness rat model. *J Biomed Mater Res Part B: Appl Biomater.* 2023;111(2):331-42. doi.org/10.1002/jbm.b.35153

[42] Kassam NA, Damian DJ, Kajeguka D, Nyombi B, Kibiki GS. Spectrum and antibiogram of bacteria isolated from patients presenting with infected wounds in a Tertiary Hospital, northern Tanzania. *BMC Res Notes.* 2017;10:1-6. doi.org/10.1186/s13104-017-3092-9

[43] Alghamdi MA. Metal-Organic Frameworks for Diabetic Wound Healing. *Cureus.* 2023;15(5). DOI: 10.7759/cureus.39557

[44] Bucknall T. Factors affecting wound-healing. *Prob Gen Surg.* 2010;6(2):194-219. doi/abs/10.1177/0022034509359125

[45] Fu L-Q, Chen X-Y, Cai M-H, Tao X-H, Fan Y-B, Mou X-Z. Surface engineered metal-organic frameworks (MOFs) based novel hybrid systems for effective wound healing: a review of recent developments. *Front Bioeng Biotechnol.* 2020;8:576348. doi.org/10.3389/fbioe.2020.576348

[46] Kondratowicz I, Shalayel I, Nadolska M, Tsujimura S, Yamagata Y, Shitanda I, Zebda A. Impact of lactic acid and genipin concentration on physicochemical and mechanical properties of chitosan membranes. *J Polym Environ.* 2023;31(3):1221-31. doi.org/10.1007/s10924-022-02691-z

[47] Biranje SS, Madiwale PV, Patankar KC, Chhabra R, Bangde P, Dandekar P, Adivarekar RV. Cytotoxicity and hemostatic activity of chitosan/carrageenan composite wound healing dressing for traumatic hemorrhage. *Carbohydr Polym.* 2020;239:116106. doi.org/10.1016/j.carbpol.2020.116106

[48] Wang X, Liu P, Wu Q, Zheng Z, Xie M, Chen G, Yu J, Wang X, Li G, Kaplan D. Sustainable antibacterial and anti-inflammatory silk suture with surface modification of combined-therapy drugs for surgical site infection. *ACS Appl Mater Interfaces.* 2022;14(9):11177-91. doi.org/10.1021/acsami.2c00106

[49] Guo S, Ren Y, Chang R, He Y, Zhang D, Guan F, Yao M. Injectable self-healing adhesive chitosan hydrogel with antioxidative, antibacterial, and hemostatic activities for rapid hemostasis and skin wound healing. *ACS Appl Mater Interfaces.* 2022;14(30):34455-69. doi.org/10.1021/acsami.2c08870

- [50] Qiao Z, Lv X, He S, Bai S, Liu X, Hou L, He J, Tong D, Ruan R, Zhang J, Ding J A mussel-inspired supramolecular hydrogel with robust tissue anchor for rapid hemostasis of arterial and visceral bleedings. *Bioact Mater.* 2021;6(9):2829-40. doi.org/10.1016/j.bioactmat.2021.01.039
- [51] Wang Y, Li X, Yuan J, Wang X, Tao K, Yan J. A bionic self-assembly hydrogel constructed by peptides with favorable biosecurity, rapid hemostasis and antibacterial property for wound healing. *Front Bioengin Biotechnol.* 2022;10:901534. doi.org/10.3389/fbioe.2022.901534
- [52] Wang W, Zhang Q, Zhang M, Lv X, Li Z, Mohammadniaei M, et al. A novel biodegradable injectable chitosan hydrogel for overcoming postoperative trauma and combating multiple tumors. *Carbohydr Polym.* 2021;265:118065. doi.org/10.1016/j.carbpol.2021.118065
- [53] Liu T, Xiao B, Xiang F, Tan J, Chen Z, Zhang X, Wu C, Mao Z, Luo G, Chen X, Deng J. Ultrasmall copper-based nanoparticles for reactive oxygen species scavenging and alleviation of inflammation related diseases. *Nature commun.* 2020;11(1):2788. doi.org/10.1038/s41467-020-16544-7
- [54] Xiao J, Chen S, Yi J, Zhang HF, Ameer GA. A cooperative copper metal–organic framework-hydrogel system improves wound healing in diabetes. *Adv Funct Mater.* 2017;27(1):1604872. doi.org/10.1002/adfm.201604872
- [55] Zhang K, Jiao X, Zhou L, Wang J, Wang C, Qin Y, Wen Y. Nanofibrous composite aerogel with multi-bioactive and fluid gating characteristics for promoting diabetic wound healing. *Biomaterials.* 2021;276:121040. doi.org/10.1016/j.biomaterials.2021.121040
- [56] Yu B, Sun W, Lin J, Fan C, Wang C, Zhang Z, Wang Y, Tang Y, Lin Y, Zhou D. Using Cu-Based Metal–Organic Framework as a Comprehensive and Powerful Antioxidant Nanozyme for Efficient Osteoarthritis Treatment. *Adv Sci.* 2024:2307798. doi.org/10.1002/advs.202307798
- [57] Jafarzadeh S, Golgoli M, Azizi-Lalabadi M, Farahbakhsh J, Forough M, Rabiee N, Zargar M. Enhanced carbohydrate-based plastic performance by incorporating cerium-based metal-organic framework for food packaging application. *Int J Biol Macromol.* 2024:130899. doi.org/10.1016/j.ijbiomac.2024.130899
- [58] Zivanovic S, Li J, Davidson PM, Kit K. Physical, mechanical, and antibacterial properties of chitosan/PEO blend films. *Biomacromolecules.* 2007;8(5):1505-10. doi.org/10.1021/bm061140p

- [59] Gomaji Chaudhary R, A Tanna J, V Gandhare N, R Rai A, D Juneja H. Synthesis of nickel nanoparticles: Microscopic investigation, an efficient catalyst and effective antibacterial activity. *Adv Mater Lett*. 2015;6(11):990-8. doi.org/10.5185/amlett.2015.5901
- [60] Song Z, Yao W, Zhang X, Dong Y, Zhang Z, Huang Y, Jing W, Sun L, Han Y, Hu F, Yuan Z. Controlled growth of metal-organic frameworks on small intestinal submucosa for wound repair through combined antibacterial and angiogenic effects. *Nano Today*. 2024;54:102060. doi.org/10.1016/j.nantod.2023.102060
- [61] Bashambu L, Singh R, Verma J. Metal/metal oxide nanocomposite membranes for water purification. *Mater Today Proc*. 2021;44:538-45. doi.org/10.1016/j.matpr.2020.10.213
- [62] Biao L, Tan S, Wang Y, Guo X, Fu Y, Xu F, Zu Y, Liu Z. Synthesis, characterization and antibacterial study on the chitosan-functionalized Ag nanoparticles. *Mater Sci Eng: C*. 2017;76:73-80. doi.org/10.1016/j.msec.2017.02.154
- [63] Ferreira MR, Gomes SC, Moreira LM. Mucoïd switch in Burkholderia cepacia complex bacteria: Triggers, molecular mechanisms and implications in pathogenesis. *Adv Appl Microbiol*. 107: Elsevier; 2019. p. 113-40. doi.org/10.1016/bs.aambs.2019.03.001
- [64] Shehabeldine AM, Salem SS, Ali OM, Abd-Elsalam KA, Elkady FM, Hashem AH. Multifunctional silver nanoparticles based on chitosan: Antibacterial, antibiofilm, antifungal, antioxidant, and wound-healing activities. *J Fungi*. 2022;8(6):612. doi.org/10.3390/jof8060612
- [65] Serbo JV, Gerecht S. Vascular tissue engineering: biodegradable scaffold platforms to promote angiogenesis. *Stem Cell Res Ther*. 2013;4(1):1-8. doi.org/10.1186/scrt156
- [66] Wu T, Hou X, Li J, Ruan H, Pei L, Guo T, Wang Z, Ci T, Ruan S, He Y, He Z. Microneedle-mediated biomimetic cyclodextrin metal organic frameworks for active targeting and treatment of hypertrophic scars. *Acs Nano*. 2021;15(12):20087-104. doi.org/10.1021/acsnano.1c07829